Social memory deficit gated by dysregulation of the cerebellar vermis

Owen Y Chao
University of Minnesota
Salil Saurav Pathak
University of Minnesota
Hao Zhang
University of Minnesota
George Augustine
Lee Kong Chian School of Medicine, Nanyang Technological University https://orcid.org/0000-0001-7408-7485
Jason Christie
University of Colorado School of Medicine
Chikako Kikuchi
Max Planck Florida Institute for Neuroscience
Hiroki Taniguchi
Ohio State University Wexner Medical Center
Yi-Mei Yang (ymyang@d.umn.edu)
University of Minnesota https://orcid.org/0000-0003-1491-8106

Article

Keywords: social memory, cerebellum, interneuron, Purkinje cell, chemogenetics, optogenetics, cFos, functional connectivity, anatomical tracing

Posted Date: March 16th, 2022

DOI: https://doi.org/10.21203/rs.3.rs-1393639/v1

Social memory deficit gated by dysregulation of the cerebellar vermis

Owen Y. Chao[1], Salil Saurav Pathak[1,#], Hao Zhang[1,#], George J Augustine[2], Jason M Christie[3], Chikako Kikuchi[4], Hiroki Taniguchi[5,6], Yi-Mei Yang[1,7,*]

[1] Department of Biomedical Sciences, University of Minnesota Medical School, Duluth, MN 55812, USA
[2] Lee Kong Chian School of Medicine, Nanyang Technological University, 308232, Singapore
[3] University of Colorado School of Medicine, Aurora, CO 80045, USA
[4] Max Planck Florida Institute for Neuroscience, Jupiter, FL 33458, USA
[5] Department of Pathology, Ohio State University Wexner Medical Center, Columbus, OH 43210, USA
[6] Chronic Brain Injury, Ohio State University Wexner Medical Center, Columbus, OH 43210, USA
[7] Department of Neuroscience, University of Minnesota, Minneapolis, MN 55455, USA
[#] These authors contributed equally
* Corresponding author
Yi-Mei Yang, PhD
Department of Biomedical Sciences
University of Minnesota Medical School
1035 University Drive
Duluth MN 55812, USA
Phone: +1 218-726-7818
Email: ymyang@d.umn.edu

Abbreviated title: Cerebellar engagement in social recognition memory

Number of words in the Summary: 210
Number of words in the Introduction, Results and Discussion: ~4900
Number of words in the Methods: ~2700
Number of figures/tables: 6 figures
Supplementary information: 2 figures and 1 table
Number of references: 86

ABSTRACT

Social recognition memory (SRM) is a key determinant of social behavior because it integrates past experiences into social interactions to distinguish familiar from novel conspecifics. The cerebellum is an important region for social functions; dysregulated cerebellar output is a common phenotype in various mouse models of autism. However, how the abnormal local activity in the cerebellum leads to social behavior deficits remains unknown. To this end, we selectively increased the excitability of molecular layer interneurons (MLIs) to suppress Purkinje cell (PC) firing with chemo- and optogenetic approaches in the mouse cerebellar vermis. Chemogenetic perturbation of MLIs impaired SRM without affecting sociability, anxiety levels, motor coordination or object recognition. Optogenetic interference of MLIs during distinct phases of a social recognition test highlighted cerebellar engagement in retrieval, but not encoding, of social information. Functional mapping with an immediate early gene product (*c-Fos*) following the social recognition test revealed that cerebellar manipulation significantly reduced brain-wide interregional correlations and shifted network structure from the medial prefrontal cortex (mPFC) and hippocampus- to amygdala-centered modules. Transsynaptic tracing showed hierarchical projections from the central cerebellum to the social brain network. Collectively, our results suggest that the cerebellum organizes the neural matrix required for SRM, providing a circuitry basis for social impairments in autism and other psychiatric disorders.

KEY WORDS: social memory, cerebellum, interneuron, Purkinje cell, chemogenetics, optogenetics, *c-Fos*, functional connectivity, anatomical tracing

INTRODUCTION

Social behavior, defined as interactions among conspecifics, is evolutionarily conserved and critical for survival of both individuals and species. Social behavior involves processes that detect, store, and respond to social stimuli, which requires the concerted actions of multiple brain areas including the medial prefrontal cortex (mPFC), anterior cingulate cortex (ACC), hippocampus, and amygdala[1-3]. Damage to any of these regions can affect social behavior, making it susceptible to pathological conditions, *e.g.*, Alzheimer's disease, schizophrenia, and autism spectrum disorder (ASD)[4-6]. Despite its significance, our understanding of the neural basis for social behavior is incomplete.

Although the cerebellum is not typically considered to be part of the social brain[1-3], it has emerged as a key node in an integrative network that links diverse functions of sense, motor, emotion, cognition and working memory[7,8]. In the cerebellar cortex, Purkinje cells (PCs) receive excitatory and inhibitory inputs and carry the sole output[9]. While synaptic excitation facilitates PC firing, the firing rates are strongly controlled by feedforward inhibition from molecular layer interneurons (MLIs)[10,11]. Nearly all PCs send GABAergic axons to inhibit the deep cerebellar nuclei (DCN)[12]. Glutamatergic neurons in the DCN directly connect to first-order targets, such as the ventral thalamus (vTH) and ventral tegmental area (VTA); and then to second-order targets virtually in the entire neocortex[13-15]. The neocortex, in turn, sends input back to the cerebellar cortex via the pontine nuclei. Through these feedback loops, the cerebellum is viewed as an estimator of the internal state for the operation of movement and cognition[16-18]. The diverse functionality of the cerebellum comes from topographical organization of the cerebellar-cortical circuits. While the anterior cerebellum (lobules I-V) is largely involved in motor coordination, the posterior cerebellum (lobules VI-IX) participates in social cognition, working memory, and language by interactions with the prefrontal, parietal, and temporal cortices[19-21]. The anterior and posterior lobes are further divided into a central vermis, intermediate paravermis, and lateral hemispheres. The vermis and its major projections to the medial DCN (mDCN) are linked to the limbic system[15]; these connections may mediate spatial memory and aggressive behavior[22-24]. Together, the extensive cerebellum-neocortex innervation provides an anatomical base for cerebellar engagement in social behavior[25].

Social interactions depend on intentions, emotions, and memories of social encounters, covering distinct yet interactive processes of social cognition and social memory[1-3]. Social cognition is the ability to imitate the actions of others (mirroring) and to understand the mental states of oneself and others (mentalizing or Theory of Mind)[1-3]. Social memory (or social recognition memory, SRM) is the ability to distinguish between familiar and novel conspecifics by recalling previous encounters; it is supported by the integrity of the hippocampus, mPFC, ACC, and amygdala[26-31]. Meta-analyses of functional magnetic resonance imaging (fMRI) studies have shown that the human cerebellum partakes in the neural networks for mirroring and mentalizing social information[32,33]. Although there is no direct evidence for cerebellar association with SRM, the cerebellum is known to encode procedural memories, most notably eyeblink conditioning[34]. Early reports indicate that MLIs contribute to consolidation of the learned eyeblink response by suppressing PC activity and releasing the DCN from tonic PC inhibition to enable the eyeblink reflex[35-37]. Interestingly, dysregulated cerebellar circuits, in which low PC activity at least partially arises from MLI over-inhibition, underlie social impairments in various mouse models of ASD[38-42]. However, it remains to be determined how the cerebellum transforms such abnormal local activity into global deficits in social behavior.

Using chemogenetic and optogenetic techniques, we phenocopied the cerebellar dysfunction observed in the ASD mouse models[38-42] by selectively increasing the excitability of MLIs to reduce PC firing in the vermis. We then evaluated the effects of these manipulations on mouse behavior. As the changes in MLI activity specifically affected SRM, we conducted functional mapping of the cerebello-cerebral axis by measuring the expression of an immediate early gene *c-Fos* after a SRM test[43]. Lastly, we traced the inter-nucleus connections from the mDCN to the cerebral cortex. Our findings indicate that MLIs finetune cerebellar intrinsic circuits to contextualize the extrinsic networks for social memory, thereby enabling normal social behavior.

RESULTS

Chemogenetic excitation of MLIs in the cerebellar vermis disrupts SRM

We used an adeno-associated virus (AAV)-mediated chemogenetic approach[44] to express an excitatory Designer Receptors Exclusively Activated by Designer Drugs (DREADD, AAV8-hSyn-DIO-hM3Dq-mCherry) in major vermal lobules of the anterior (vermis IV/V) or posterior (vermis VI/VII) cerebellum of adult c-kit$^{IRES\text{-}Cre}$ mice (**Fig. 1a**). Via Cre-LoxP recombination, the *c-kit* promoter allows selective transduction of MLIs postnatally[45]. The vermis was targeted because of its topographical connection to the limbic system and its consistent association with neuropsychiatric disorders[15]. To examine transduction efficiency, we imaged cerebellar sections several weeks after viral infusions and behavioral tests. Robust yet localized expression of the hM3Dq receptor (marked with mCherry) in lobule IV/V or VI/VII was observed (**Fig. 1b**). Higher-resolution imaging revealed that hM3Dq expression was predominantly in MLIs (**Fig. 1b**). Among MLIs, stellate cells (SCs) innervate the distal dendrites of PCs and do not directly affect PC firing[46], whereas basket cells (BCs) execute powerful inhibition of PC activity by forming GABAergic synapses on the soma and ephaptic connections on the axon initial segment of PCs[10]. Thus, we validated our ability to chemogenetically modulate MLI activity by *ex vivo* patch-clamp recordings from BCs. Activation of the hM3Dq with clozapine-N-oxide (CNO; 10 μM) significantly increased the frequency of action potentials (APs) in BCs expressing the excitatory DREADD (p=0.011) but had no effect on non-transduced BCs (p>0.05) (**Fig. 1c** & **1d**; statistical details in **Supplementary Table 1**).

Next, we evaluated the impact of the chemogenetic excitation of MLIs on mouse behavior by intraperitoneal (i.p.) injection of CNO (1 mg/kg) 30-40 min before each assay[41,47]. Compared to their littermate controls that lacked Cre recombinase, c-kit$^{IRES\text{-}Cre}$ mice transduced with the excitatory DREADD in lobule IV/V or VI/VII showed no differences in open-arm avoidance (measured with an elevated plus maze test), locomotion (measured with an open field test), motor coordination (measured with a rotarod test), or social play (measured with a reciprocal social interaction test) (**Supplementary Fig. 1**), largely in line with previous reports that interfering the output activity of the vermis in adult mice did not affect their general performance[41,47,48]. To further scrutinize their social behavior, we conducted a three-chamber social test that consisted of a sociability trial immediately followed by a social novelty trial (**Fig. 1e**)[49]. In the sociability trial, all groups explored the stranger mouse more than the empty cup (control: p=0.005,

vermis IV/V: p=0.008, vermis VI/VII: p=0.020; paired t-test) and rendered positive sociability indices (one sample t-test) (**Fig. 1e**, **top**). In the social novelty trial, both control mice and those expressing the DREADD in vermis IV/V explored the new stranger more than the old one (p=0.031 and 0.022, respectively), while the mice expressing the DREADD in vermis VI/VII did not show such a preference (p>0.05), resulting in a social novelty index near 0 (**Fig. 1e**, **bottom**).

Social novelty preference relies on remembering previous encounters and is driven by seeking the unknown[50]. To determine whether the lack of social novelty preference was caused by memory loss, we performed a social recognition test with a prolonged interval (45 min) between a learning and a testing trial (**Fig. 1f**). The time delay was introduced to assess memory retention[26]. In the learning trial, all animals displayed normal social tendency toward the stranger mouse (control: p=0.01, vermis IV/V: p=0.005, vermis VI/VII: p=0.012) and had positive social learning scores (**Fig. 1f**, **top**), consistent with findings from the three-chamber social test (**Fig. 1e**). In the testing trial, the control group again showed intact social novelty preference (p=0.002). However, the vermis-perturbed groups explored the new and the old strangers indiscriminately (p>0.05), accompanied with low social recognition scores (**Fig. 1f**, **bottom**). To determine whether the chemogenetic perturbation reduced memory capacity or motivation to seek novelty in general, we did an object recognition test, which was identical to the social recognition test except that the social stimuli were replaced with inanimate objects (**Fig. 1g**). Surprisingly, all groups spent more time exploring the novel object than the old object (control: p=0.019, vermis IV/V: p=0.009, vermis VI/VII: p=0.012) with positive object recognition scores (**Fig. 1g**), indicating well-preserved object-based memory and novelty-seeking behavior. The total exploration time between groups was comparable in all the tests (**Supplementary Table 1**). Taken together, these findings suggest that the cerebellar vermis is important for SRM without affecting anxiety levels, locomotion, exploratory motivation, social approaching, or object recognition memory in animals.

Optogenetic stimulation of MLIs in the vermis interferes with retrieval, but not encoding, of SRM

SRM is a type of declarative memory that consists of encoding, storage/consolidation, and retrieval of social information[51]. To specify at which of these stages the cerebellum is engaged, we employed an

optogenetic approach that permits precise temporal control of neuronal firing[52]. We chose a bacterial artificial chromosome (BAC) transgenic mouse line that uses the *nNOS* promoter to express channelrhodopsin-2 (ChR2) in MLIs (nNOS-ChR2)[53]. Consistent with a previous report[53], ChR2 (fused to YFP) was expressed in most MLIs in the adult cerebellum (**Fig. 2a**). Co-labeling PCs with an anti-Calbindin antibody confirmed that ChR2 was exclusively present in the somas, dendrites, and axon terminals of MLIs (**Fig. 2a**). To measure neuronal responses to optogenetic photostimulation, we recorded APs from MLIs (BCs) and PCs while delivering an 8 Hz train of light pulses (470 nm, 25 ms duration) (**Fig. 2b**). This low frequency ensures reliable generation of MLI APs in response to light flashes[53]; and it falls within the range of theta oscillations (4-10 Hz), which play a central role in learning and memory[54]. Specifically, theta-burst stimulation of the human cerebellum affects episodic memory[55]. As shown in **Fig. 2b-2d**, photostimulation rapidly increased AP frequency in MLIs (p=0.018; paired t-test), while reducing AP firing in postsynaptic PCs (p=0.005). Upon cessation, MLI and PC activity returned to baseline levels. In addition, the light stimuli decreased regularity of AP firing in PCs, indicated by an increase in the coefficient of variation (CV) of inter-AP-intervals (p<0.001) (**Fig. 2d**).

Applying the same light pulses through optic fibers implanted in lobule IV/V or VI/VII, we studied the behavior consequences of photostimulating MLIs. In an open field test, nNOS-ChR2 mice and their littermate controls (not expressing ChR2) traveled a similar distance, and the light stimulation did not change their locomotor activity (p>0.05; **Supplementary Table 1**). To know how the vermis was involved in the process of SRM, we photostimulated in different sessions of a social recognition test. When the light was presented during the learning trial (**Fig. 2e**), all mice explored the stranger more than the empty cup (control: p=0.006, vermis IV/V: p=0.008, vermis VI/VII: p=0.001; paired t-test) with positive social learning scores (one sample t-test) (**Fig. 2e**, **top**). They also explored the novel stranger more than the familiar one (control: p=0.012, vermis IV/V: p=0.004, vermis VI/VII: p=0.042) with positive social recognition scores (**Fig. 2e**, **bottom**). Perturbing lobule IV/V yielded less exploration in total as compared to the other groups (**Supplementary Table 1**), which may reflect deficits in motivation, attention and/or sensorimotor integration associated with interference of the anterior cerebellum[47].

Overall, perturbation of the cerebellum at the encoding stage did not impair sociability, social novelty preference or SRM.

In contrast, when the light was presented during the testing trial (**Fig. 2f**), all mice spent more time exploring the stranger than the empty cup (control: $p<0.001$, vermis IV/V: $p=0.003$, vermis VI/VII: $p=0.045$) with positive indices of sociability (**Fig. 2f**, **top**). Yet, unlike the control group that explored the novel stranger more than the old one ($p=0.008$), the vermis-perturbed groups did not prefer the novel stranger ($p>0.05$), leading to poor indices of social recognition (**Fig. 2f**, **bottom**). Because there was no group difference in total exploration in this case ($p>0.05$; **Supplementary Table 1**), the loss of social recognition was likely accounted for by an inability to recall previous encounters while vermal MLIs were activated rather than by confounding factors such as a lack of inquisitiveness. When the light stimulation was applied in the testing trial of an object recognition test (**Fig. 2g**), all animals preferred the new object to the old one (control: $p=0.033$, vermis IV/V: $p=0.052$, vermis VI/VII: $p=0.035$) with positive indices of object recognition (**Fig. 2g**), implying a minimal effect of this manipulation on non-social recognition memory. These results suggest that the cerebellum plays a specific role in the retrieval (or consolidation), but not the encoding, of social information.

Perturbing the vermis decreases functional connectivity and disorganizes network structure of brain regions essential for SRM

To understand how the cerebellum mediates SRM, we monitored neuronal activity via a molecular marker, *c-Fos*, in 24 brain regions following the social recognition test on c-kit$^{IRES\text{-}Cre}$ mice and their littermate controls (**Fig. 3a**). As shown in **Fig. 1f**, activation of vermal MLIs by the excitatory DREADD disrupted SRM. 90 min after the test, we collected brain tissue for *c-Fos* immunostaining. Basal levels of *c-Fos* are normally low[56] but are elevated by external stimuli, making this immediate early gene a useful tool to identify activated neurons[43]. The 90-min window was chosen because *c-Fos* expression peaks 1-2 hours after stimulation[57]. We examined *c-Fos* expression in brain regions with well-established roles in SRM[26-31]. By counting the number of *c-Fos*-positive cells in each region and normalizing these values to the mean number of *c-Fos*-positive cells in the control group, we found

significant effects on *c-Fos* levels for the mPFC, parahippocampal cortices, amygdala, hypothalamus and VTA (p<0.05; one-way ANOVA; **Supplementary Fig. 2** & **Table 1**). Perturbing the vermis, irrespective of the lobules, elevated *c-Fos* expression in the temporal association cortex (TeA), ectorhinal cortex (Ect), and perirhinal cortex (PRh) compared to the control group (p<0.05; Fisher's LSD; **Supplementary Fig. 2**). These parahippocampal cortices interact with the hippocampus and cerebral cortex to support high-order cognitive processes such as contextual associations and emotional inferences[58]. In other regions, changes in *c-Fos* depended upon which lobule was targeted. For instance, perturbing lobule IV/V mostly reduced *c-Fos* levels in subdivisions of the mPFC (anterior cingulate cortex (rostral), Acg: p=0.024; prelimbic cortex, PL: p=0.044; but not infralimbic cortex, IL: p>0.05; **Fig. 3b**). In contrast, perturbing lobule VI/VII increased *c-Fos* levels in subdivisions of the amygdala (central nucleus of amygdala, CeA: p=0.003; basolateral amygdala, BLA: p=0.007; but not basomedial amygdala, BMP: p>0.05; **Fig. 3c**). The differences are likely related to distinct connections of the anterior and posterior vermis to the subcortical and cortical regions[19-21].

To gain insight into functional connectivity, we calculated Pearson correlation coefficients (r) of each pair of brain regions across the subjects in each group based on the *c-Fos* measurements. We then created interregional correlation matrices with the values of Pearson's r from 1 to -1 indicated by a gradient spectrum from red to indigo, respectively (**Fig. 4a**). As the matrices exhibited discrete patterns for each group, we further analyzed the network connectivity by only including the most positive (r>0.6) and the most negative (r<-0.6) correlations in the network plots (**Fig. 4b**). The plots comprised the brain regions (nodes) and their connections (edges; red lines: r>0.6, indigo lines: r<-0.6). A chi-square test revealed that the control group had more edges, and proportionally more positive correlations, than the vermis-perturbed groups (vermis IV/V: χ^2=66.03, p<0.001, vermis VI/VII: χ^2=27.42, p<0.001; **Fig. 4c**). Perturbing the vermis substantially reduced the mean r of all the brain regions in comparison to the control group (vermis IV/V: p<0.001, vermis VI/VII: p=0.001; **Fig. 4d**), implying a decrease in concerted brain-wide activity. **Fig. 4e**-**4h** highlighted four key regions underpinning SRM. Both vermis groups had lower r than the control group in the mPFC, ACC, and hippocampus (p<0.05 for all; Fisher's LSD), except that the difference for the vermis VI/VII group in the ACC was not significant (p=0.087).

Conversely, the vermis groups had higher *r* than the control group in the amygdala although the increase of the vermis IV/V group was mild (p=0.069); this may reflect the lobule-specific changes of *c-Fos* expression observed in the amygdala (**Fig. 3c**).

To define network properties, we did graph theoretical analysis by focusing on the positive correlations in the matrix of each group. First, we computed degree (the number of edges that a node has) and betweenness (the number of shortest paths that pass through a node) to assess the centrality of a network node. A high value for "degree" indicates a brain region that is connected to many others, and a high "betweenness" indicates a brain region that has close control over other regions[59,60]. For degree, the Ect, hippocampus (CA1 and dentate gyrus [DG]), and primary motor cortex (M1) were ranked high (>0.8) in the control group, while the amygdala (BLA and BMP), parietal association cortex (PtA), lateral entorhinal cortex (lEnt), and Acg were ranked high in the vermis groups (**Fig. 5a-5c**, **left**). For betweenness, the Ect and TeA were ranked high (>0.8) in the control group, while the PtA and Acg were ranked high in the vermis groups (**Fig. 5a-5c**, **middle**). Next, we quantified within-community *Z*-scores (the extent of a node connected in its own community) and participation coefficients (the extent of a node connected to other communities) to outline the modularity of the network. A brain region with high rankings in both *Z*-score and participation coefficient is classified as a connector hub that regulates the interactions within and between communities (modules)[59,60]. In the control group, the Ect, TeA, hippocampus (CA1, CA2/3 and DG), mPFC (Acg and IL), M1, and ACC had high ranks for both *Z*-scores and participation coefficients, whereas in the vermis groups, the amygdala (BLA and BMP), PtA, lEnt, Acg, and VTA had high ranks for *Z*-scores, but their participation coefficients were zero (**Fig. 5a-5c**, **right**). Lastly, we simulated the spatial distribution of the degree and betweenness centralities in a force atlas format, where distinct modules were color-coded. The control group contained two highly interactive modules (**Fig. 5d**). One module (pink) was centered on the hippocampus and mPFC, which are involved in cognitive and emotional regulation of mnemonic processes[50]. The other module (green) included the parahippocampal cortices and CA2/3, which play a role in integrating sensory information for memory establishment[27,58]. Perturbation of the vermal lobules destroyed these modules and produced solitary, amygdala-centered networks (**Fig. 5e-5f**). Given that dynamic interactions among

the amygdala, hippocampus, parahippocampus and mPFC are crucial for emotion-based memory[61,62], we propose that the cerebellum supports SRM by promoting and coordinating functional connectivity of the corticolimbic system.

Anatomical tracing of the medial cerebellar nucleo-cortical connections

The vermis and paravermis influence the corticolimbic system through projections to the mDCN (fastigial and interposed nuclei)[15]. To track the ascending connections of the mDCN to the neocortex, we injected AAV1-hSyn-Cre unilaterally into the mDCN of floxed tdTomato mice[63] (**Fig. 6a**). Cre-LoxP recombination labeled axons of mDCN neurons, allowing identification of first-order targets of these cells. Because AAV1-hSyn-Cre has an anterograde transsynaptic property[64], this experiment further allowed us to follow axons of the first-order neurons to second-order stations. We targeted neurons in the fastigial (mostly) and interposed nuclei while largely avoiding the dentate nucleus (**Fig. 6b**). Then we traced downstream projections contralateral to the injection site in the 24 brain areas that were examined for *c-Fos* expression (**Fig. 4**).

We found cell bodies and processes of labeled neurons in the first-order nuclei including the vTH and VTA across individual mice (n=3) (**Fig. 6c**, **left**). This is consistent with previous reports on the monosynaptic connections between the DCN and these regions, as well as the involvement of these connections in social behavior[65,66]. Beside the vTH (ventrolateral and ventromedial thalamus), neurons in the centrolateral, parafascicular, mediodorsal, and ventral posteromedial thalamus, were strongly labeled (**Fig. 6c**, **right**), in line with recent anatomical studies[67,68]. Moreover, we observed neurons expressing tdTomato sparsely distributed in the dorsomedial and lateral hypothalamus. The cerebellar-hypothalamic contacts may be important for somatic and visceral integration[69-71]. Among the second-order nuclei, robust axon (not soma) labeling was apparent in subcortical regions, *e.g.*, the dorsal striatum (dSTR) and nucleus accumbens (NAc) (**Fig. 6d**, **left**). But labeling was absent in the hippocampus and amygdala (**Fig. 6d**, **left**), confirming a lack of mono- or disynaptic innervation from the fastigial nuclei to these areas[67]. The engagement of hippocampus and amygdala in the cerebellum-mediated SRM (**Fig. 5**) is likely through their intense crosstalk with other brain regions, such as the

cerebral cortex[72,73], that are connected to the DCN[67,68]. In fact, we observed a great number of labeled axons in the somatosensory cortex (S1 and S2), somatomotor cortex (M1) and PtA as well as moderate labeling in the Ect, mPFC (Acg, PL and IL) and ACC (**Fig. 6d**, **right**). These data provide anatomical structures for cerebellar regulation of SRM. However, the functional connectivity for each region derived from the *c-Fos* mapping (**Fig. 3**-**5**) does not simply correlate to its structural connection with the medial cerebellum (**Fig. 6**), which implicates the complexity of the inter-nucleus circuits subserving SRM.

DISCUSSION

By manipulating cerebellar activity with spatiotemporal control, we have uncovered a new role for the cerebellum in incorporation of working memory into social behavior. Specifically, we found that activating MLIs in the vermis during memory recall impaired social, but not non-social, recognition memory. Neuroanatomical tracing and c-*Fos* functional mapping revealed the circuitry basis for the cerebellum to co-activate and coordinate the limbic structures essential for emotional responses and cognitive functions in support of SRM. This work provides evidence for the internal forward model, in which the cerebellum conducts mental activity by orchestrating the cerebellar-cortical network[16-18].

Although the cerebellum is known for motor coordination, our manipulations did not affect animals' motor performance on the accelerating rotarod or exploratory activity in less challenging conditions, *e.g.*, in the open field (**Supplementary Fig. 1**). This can be for several reasons. First, our interference was restricted to a single lobule, as indicated by the localized expression of hM3Dq in **Fig. 1**. Activation of MLIs in a lobule might be insufficient to disturb general movements, even though it was sufficient to produce a SRM deficit. The sensitivity of the non-motor function to the cerebellar interference is congruent with other studies using similar approaches[23,24,48]. Second, we manipulated MLIs instead of PCs to attenuate, rather than silence, the output of the cerebellar cortex (**Fig. 1** & **2**). This tactic helped minimize potential alterations in locomotor skills, anxiety levels, and social preference that could confound the assessment of SRM[50]. Lastly, the subregions that we perturbed are known to be less involved in online motor control. While the anterior vermis may be part of the sensorimotor representation[20] and targeting lobule IV/V with photostimulation occasionally impeded exploratory

behavior (**Fig. 2e**), the posterior vermis typically represents cognitive functions[19-21] and interfering with lobule VI/VII had no effect on total exploration time in the object and social recognition tests (**Fig. 1** & **2**). Although these two tests had the same structure, vermis-perturbed animals were able to discriminate between objects by spending more time on the new object than the old one yet failed to show such a preference in identifying conspecifics. This demonstrates an explicit contribution of the cerebellum to SRM, independent of confounding factors such as reduced motor ability, motivation, or interest in novelty.

We focused on the role of MLIs in SRM because they actively participate in learning and memory to define motor and non-motor functions by spatially and temporally tuning PCs in the circuits[10,11]. For example, blocking MLI-PC synaptic transmission with a GABA receptor mutation impairs consolidation of vestibulo-cerebellar motor learning and expression of eyeblink conditioning[36,74]. Optogenetic excitation of MLIs in the floccular lobe alters adaptation of the vestibulo-ocular reflex[75]. Chemogenetic inhibition of MLIs in paravermal lobule VI or crus 1 leads to deficient eyeblink conditioning responses[48]. The same manipulation in lobule VI affects reverse learning and in lobule VII affects novelty-seeking behavior, signifying a role of MLIs in cognitive and social development beyond the motor domain. However, most of the effects are present in juvenile mice and diminish when animals reach maturity[48]. Our manipulation of MLIs in the adult mice also had little effect on learning, emotion, or sociability (**Supplementary Fig. 1**) except for SRM (**Fig. 1** & **2**). This unexpected finding may be due to our experimental design. Opposite to suppressing MLIs[48], we increased their activity based on a common phenotype among ASD mouse models[38-42]. Thereby, we demonstrated the significance of MLIs in social interactions, although determination of how these neurons encode SRM requires further investigation with *in vivo* recordings of APs or Ca^{2+} signals from MLIs during social recognition tasks.

The performance of SRM exploits working memory while judging a recently encountered conspecific[26-31]. Cerebellar involvement in working memory is well documented in human and animal studies[13-15]. Schmahmann and Sherman first reported patients with damages to the posterior lobe and the vermis displayed working memory loss along with other cognitive and affective symptoms[76]. Work from animal models has begun to reveal the mechanisms. Interfering with PC activity does not affect

object recognition memory *per se*, like our data in **Fig. 1** & **2**, but compromises location- or sequence-based memory via the cerebellum-hippocampus connectivity[23,77]. Moreover, the cerebellum participates in decision-making and consolidation of reward-related go/no-go memory tasks[78-80]. As social interactions are rewarding[81], the cerebellum may promote SRM through its connections to the reward pathway[65], which significantly overlap with the social brain network[1-3].

We constructed the *c-Fos*-derived neural network underlying SRM and identified two main modules centering on the mPFC-hippocampus and Ect-TeA (**Fig. 3**-**5**). The mPFC-hippocampus module may be essential for processing episodic information of "what", "where" and "when"[50]; and the Ect-TeA module may be critical for integrating sensory information into the mPFC-hippocampus memory system[58]. Perturbing the cerebellum broke down the highly interactive clusters and shifted the brain network to an amygdala-centered module (**Fig. 5**). The emergence of amygdala as a hub reinforces our results that the vermis is of particular importance for emotion-related memory (**Fig. 1** & **2**), likely via its preferential connections to the limbic system[15]. We detected cerebellar projections in the cerebral cortex including mPFC and ACC, and in subcortical areas such as the parahippocampus and dopamine pathways (**Fig. 6**). However, we did not find mono- or disynaptic connections to the hippocampus and amygdala. The functional connectivity of these two key nodes with the cerebellum may be mediated by their interplay with the cerebral cortex[72,73]. A new study proposes that the cerebellum regulates coherence of gamma oscillations between mPFC and hippocampus for spatial memory[82]. It is tempting to speculate that the cerebellum may impact hippocampal activity in a similar way to enable SRM. The amygdala interacts with the mPFC, parahippocampus and hippocampus to modulate the effects of emotion on memory[61,62]. The fact that cerebellar perturbation can functionally alter these distal regions supports our view that the cerebellum is an integral part of the cerebello-cortical network for SRM.

Our data suggest that the cerebellum is necessary for retrieval, but not encoding, of SRM (**Fig. 2**). Memory encoding is the act of storing external features and internal states in a subset of neurons (engram) across various brain regions. Memory retrieval requires concurrent reactivation of the engram cells[51]. The neuronal activity in these two processes may differ. For instance, the hippocampal CA2/3 and DG are only active during memory formation while the subiculum (and CA1 to a less degree) is

active during memory recall[83,84]. This selective activation in the initial learning may explain why *c-Fos* expression in the hippocampus was insensitive to the changes in later performance of memory retrieval (**Supplementary Fig. 2**). In addition to recollection of contextual cues, recognition memory entails familiarity for acquaintance-based discrimination[85]. While recollection involves the medial temporal lobe including parahippocampus and amygdala, familiarity involves the PRh. Remarkably, *c-Fos* expression in all the regions was elevated by the vermal perturbation that led to the SRM deficit (**Supplementary Fig. 2** & **Fig. 3**). This strengthens the specificity of the identified neural network for recognition memory. Lastly, recall of SRM needs coactivation of engram cells in multiple regions[30,51]. Our finding that locally interfering with the vermis decreased brain-wide functional connectivity (**Fig. 4**) indicates a unique position of the cerebellum in reinstatement of memory traces by coactivating the engrams.

The results of this study must be interpreted with caution due to several technical issues. First, the readouts of *c-Fos* expression have a modest temporal resolution. Despite being a validated tool[43], *c-Fos* expression is a slow transcriptional process and does not allow real-time monitoring of neural activity or resolve the differences between events occurring close in time. Thus, the *c-Fos*-based neural network may reflect interwound responses to encoding and recalling of SRM. Further inquiry using *in vivo* electrophysiology and Ca^{2+} imaging is needed to address how the engram cells are recruited and reactivated in a task-related manner with temporal accuracy. Second, the conceptualized network model of SRM inevitably embeds other information, such as the sensory and motor processing during the social recognition task as well as environmental factors, *e.g.*, fear or stress from experimental handlings. To minimize the variables, all groups were tested under the same conditions and *c-Fos* counts were normalized to the average value of the control group for each brain region (**Fig. 3-5**). Thereby, the network disruption may largely result from the cerebellar interference. Lastly, it is worth noting that the chemo- and optogenetic manipulations are artificial, from which we can infer what the cerebellum is capable to do but not exactly what it does physiologically.

Notwithstanding these considerations, our study presents the first evidence for a causal link of the cerebellum to social memory, which advances our understanding of the neural substrates for social behavior. As social impairments are commonly associated with neuropsychiatric disorders[4-6], our

results will help develop diagnostic and therapeutic strategies by targeting cerebellar modulation of the higher-order functions with cell-type- and region-specific precision.

ACKNOWLEDGMENTS

This study was supported by the National Institute of Neurological Disorders and Stroke (NINDS) of the National Institutes of Health (NIH) grants R15 NS112964 to YMY and R01 NS112289 to JMC, the Singapore Ministry of Education grant MOE2017-T3-1-002 to GJA, the Brain & Behavior Research Foundation Young Investigator grant to OYC, and the Winston and Maxine Wallin Neuroscience Discovery Fund to YMY. AAV8-hSyn-DIO-hM3Dq-mCherry was generated by Dr. Ezequiel Marron Fernandez de Velasco in the University of Minnesota Viral Vector and Cloning Core. AAV1-hSyn-Cre was purchased from Addgene (a gift from Dr. James M Wilson). We thank Dr. Pei Wern Chin (Nanyang Technological University) for providing critical input.

AUTHOR CONTRIBUTIONS

OYC and YMY designed the project, performed the experiments, and analyzed the data with assistance from SSP and HZ. GJA, JMC, CK and HT provided the mouse lines and technical input. OYC and YMY wrote an early version of the manuscript and all other authors contributed to the final edition.

DECLARATION OF INTERESTS

The authors declare no competing financial interests.

DATA AVAILABILITY

All the data and materials are available upon request to Dr. Yi-Mei Yang (ymyang@d.umn.edu).

METHODS

Subjects

C-kit$^{IRES\text{-}Cre}$ mice and nNOS-ChR2 BAC mice were provided by Hiroki Taniguchi (Ohio State University, USA)[45] and George J Augustine (Nanyang Technological University, Singapore)[53], respectively. Ai9 (RCL-tdT) mice (stock #007909) were purchased from Jackson Laboratory (Bar Harbor, ME)[63]. Both sexes (8-12 weeks old) were included, and no sex differences were observed. Mice were kept under a 12-hour light-dark cycle (light on from 07:00 to 19:00) and reared 3-5 per cage with food and water *ad libitum*. All procedures were approved by the Institutional Animal Care and Use Committee (IACUC) and the Institutional Biosafety Committee (IBC) of University of Minnesota, in accordance with the National Institutes of Health guidelines. Heterozygous c-kit$^{IRES\text{-}Cre}$ were bred to obtain mice with or without Cre recombinase (control). Genotyping for c-kit$^{IRES\text{-}Cre}$ was done with 2 primers: 5'-CGGTCGATGCAACGAGTGATG-3' and 5'-AGCCTGTTTTGCACGTTCACC-3'. Male nNOS-ChR2 were crossed with female C57BL/6J to obtain wild-type (control) or nNOS-ChR2 mice. Genotyping was done with 2 primers: 5'-AGTAGCTCAGGTTCCTGTGGG-3' and 5'-GCAAGGTAGAGCATAGAGGG-3'.

Stereotactic Surgery

c-kit$^{IRES\text{-}Cre}$, nNOS-ChR2 and their littermate controls were randomly assigned to vermis IV/V and VI/VII surgical groups. Animals were anesthetized with a cocktail of ketamine and xylazine (100 and 10 mg/kg, respectively, i.p.). Carprofen (5 mg/kg, s.c.) was administered as an analgesic. Mice were fixed on a stereotactic frame (Stoelting, Wood Dale, IL) and an incision was made to expose the skull. For viral infusion, a hole was drilled above the cerebellum of c-kit$^{IRES\text{-}Cre}$ mice and their wild-type littermates according to the coordinates: AP: -6.0 or -7.0 mm (for vermis IV/V or VI/VII, respectively), ML: ±0.0 mm, relative to bregma[86]. AAV8-hSyn-DIO-hM3Dq-mCherry (titers >$3.0x10^{13}$, 0.1-0.15 µl, University of Minnesota Viral Vector and Cloning Core) was infused into the cerebellum (DV: -1.0 mm) with a 10-µl Hamilton syringe controlled by a microinjection pump (QSI 53311, Stoelting) at a flow rate of 0.09 µl/min. After infusion, the needle was left in place for >7 min and then slowly retracted. The wound was sutured and disinfected with 70% ethanol and iodine. For optic-fiber implantation, a hole was drilled above the cerebellum of nNOS-ChR2 mice and their wild-type littermates according to the coordinates: AP: -6.4 or -7.0 mm (for vermis IV/V or VI/VII, respectively), ML: ±0.0 mm, relative to bregma[86]. An optic

fiber (∅200 μm) attached with a ceramic ferrule (FT200EMT and CFLC230-10, Thorlabs, Newton, NJ) was implanted in the hole 0.0-0.2 mm below the cerebellum surface. Two screws and dental cement were applied to secure the optic fiber on the skull. For neuronal tracing, AAV1-hSyn-Cre (a gift from Dr. James M Wilson, plasmid #105553, titer >1x10^{13} vg/ml, Addgene, Watertown, MA) was unilaterally infused into medial deep cerebellar nuclei (mDCN) of Ai9 (RCL-tdT) mice according to the coordinates: AP: -6.2 mm, ML: 0.7 mm, DV: -2.0 mm, relative to bregma[86]. After operations, mice were placed on a heating pad (37°C) to maintain body temperature until awake. Electrophysiology and behavioral tests were conducted 3 weeks after surgeries. Imaging of labeled neurons was done 4-5 weeks after surgeries. Mice (n=1-2/group) were excluded when injections were outside the intended areas.

Electrophysiology

c-kit$^{IRES-Cre}$ mice (n=4) injected with AAV8-hSyn-DIO-hM3Dq-mCherry in vermis IV/V and nNOS-ChR2 mice (n=3) were used for electrophysiology. Following decapitation, the brain was immediately dissected, and sagittal cerebellar slices were sectioned at a thickness of 300 μm using a vibratome (VT1200S, Leica Biosystems, Buffalo Grove, IL) in ice-cold modified artificial cerebrospinal fluid (ACSF). It contained (in mM): sucrose (217.6), KCl (3), glucose (10), NaH_2PO_4 (2.5), $NaHCO_3$ (26), $MgCl_2$ (2), and $CaCl_2$ (1), continuously bubbled in 95% O_2 and 5% CO_2 (pH 7.4). Slices were then incubated in oxygenated standard ACSF including (in mM): NaCl (125), KCl (2.5), glucose (10), NaH_2PO_4 (1.25), sodium pyruvate (2), myo-inositol (3), ascorbic acid (0.5), $NaHCO_3$ (26), $MgCl_2$ (1), and $CaCl_2$ (2) (pH 7.4) at 37°C for 30 min prior to experimentation. Slices were transferred to a recording chamber mounted on a BX51WIF Olympus microscope with a 60x water immersion objective. They were perfused with the standard ACSF at a rate of ~1 ml/min. Purkinje cells (PCs) and molecular layer interneurons (MLIs) were identified by their size and location. Patch electrodes had resistances of 2.5-3 and 4.5-6 MΩ for PCs and MLIs, respectively. Action potentials (APs) at the soma were recorded in the cell-attached mode with GΩ seal at -60 mV for PCs and -70 mV for MLIs. Intracellular solution contained (in mM): K-gluconate (97.5), KCl (32.5), EGTA (0.1), HEPES (40), $MgCl_2$ (1), ATP (2), GTP (0.5) (pH 7.3). All recordings were acquired on-line at 35°C, filtered at 4 kHz, digitized at 50 kHz with a

dual-channel amplifier (MultiClamp 700B, Molecular Devices, San Jose, CA) and digitizer (Digidata 1550B, Molecular Devices). Data were analyzed off-line with MiniAnalysis 6.0.7 (Synaptosoft, Fort Lee, NJ), Clampfit 10 (Molecular Devices) and Excel 2016 (Microsoft, Redmond, WA). To activate hM3Dq receptor, clozapine-*N*-oxide (CNO, 10 µM, BML-NS105, Enzo Life Sciences, Farmingdale, NY) was applied to slices[41]. To excite channelrhodopsin 2 (ChR2), 470-nm LED light (LEDD1B, Thorlabs) was delivered through the 60x objective coupled with a GFP filter cube (Olympus)[53]. Light pulses were controlled using pCLAMP 10 (Molecular Devices). Light intensity (maximus=8.2 mW/mm^2 at the tissue) was measured with a PM100D power meter and a S121C photodiode sensor (Thorlabs).

Behavioral Testing

Either in chemogenetic (using c-kit$^{IRES\text{-}Cre}$) or in optogenetic (using nNOS-ChR2) experiments, three groups (n=7-9 mice with 3-5 females/group) were included: control, vermis IV/V, and vermis VI/VII. For chemogenetic experiments, CNO was administered in all groups (1 mg/kg, i.p.) 30-40 min prior to each test. CNO was stored in aliquots at -20°C. It was diluted in saline, kept on ice, and protected from light while in use. For optogenetic experiments, only open field, object recognition and social recognition tests were conducted. Light pulses were generated with a Polygon DMD pattern illuminator (Mightex, Toronto, Canada) powered by 470-nm LED through a cable connected to the optic fiber implanted on the animal's head. Light intensity (maximus=5.9 mW/mm^2 at the tissue) was measured with a PM100D power meter and a S121C photodiode sensor (Thorlabs).

Apparatus

An elevated plus maze consisted of a central platform (5 x 5 cm), two walled arms (25 x 5 x 25 cm) and two arms without walls (25 x 5 cm) in the shape of a cross. It was elevated 30 cm high, and the two types of arms were situated opposite to each other. A digital rotarod (Rotamex, Columbus Instruments, Columbus, OH) was used to test motor coordination. A box composed of 3 chambers (20 x 40 x 30 cm each) with passages (5 x 5 cm) within the walls that divided the chambers was used for three-chamber social tests. A box (40 × 40 × 30 cm) made of polyvinyl chloride was used for open field, object recognition, social recognition, and reciprocal social interaction tests. Different sets of objects with

variable textures (smooth or rough), sizes (diameter 7-9 cm, height 14-17 cm) and shapes (column, irregular) were used for object recognition. Objects were weighed enough to prevent being moved by animals. Assignment of objects was counterbalanced to minimize object and/or place preference. Age-, sex-, and strain-matched wild-type mice served as strangers for social tests. Metal grid cups (diameter 10 cm, height 12 cm) were used to constrain strangers. Placement of strangers was counterbalanced between subjects. All tests were done in a quiet room (<40 dB) under dim light (~50 lx) during 10:00-16:00. Test designs were based on previous studies using similar experimental protocols[41,42,47]. Apparatus was cleaned with 70% ethanol between subjects. A camera was connected to a computer to record and analyze behavior via tracking software (ANY-maze, Stoelting). Object and social exploration were manually counted by experimenters who were blind to the design. Other measurements were automatically made with the ANY-maze software.

Elevated plus maze

This test was used to assess anxiety-like behavior. A subject was placed onto the central platform (facing an open arm) and allowed to freely explore for 5 min. Entries to the center, open and closed arms, time spent in these areas, and time spent on head-dip and body-extension were analyzed.

Open field

This test was used to assess locomotor and exploratory activity. A subject was put into the center of the open field and monitored for 10-15 min. Traveling distance and duration, rearing, grooming, thigmotaxis, and center stay (virtual central square 13.3 × 13.3 cm) were analyzed in 5-min time bins.

Rotarod

This test was used to assess motor coordination and motor learning. A subject was placed on a rotarod rotating at a speed of 4 rpm until it could stay on for >1 min. Then, the speed accelerated from 4 to 40 rpm in 5 min, which was taken as one trial. 3 trials were conducted with an inter-trial interval of 15 min. Rotating speed and time staying on the rotarod before falling were recorded.

Reciprocal social interaction

This test was used to assess pro-social behavior in a native situation without physical barriers. A subject was placed into the open field along with a stranger for 10 min. An interaction was defined as

the animal' head being in physical contact with any body part of the other's, except for the tail. Duration of physical contacts was recorded.

Three-chamber social test

This test was used to assess social and social novelty preferences. It consisted of 3 sessions: habituation, sociability, and social novelty (9 min each). In the habituation trial, a subject was placed into the middle chamber and allowed to freely explore the whole apparatus. In the sociability trial, a stranger that had never been contacted by the subject was put underneath the cup in one of the side chambers. An identical empty cup was placed on the other side. In the social novelty trial, another stranger was put underneath the previously empty cup. Physical contact around the cups by the subject's nose, head and forelimbs was defined as explorative behavior. Sociable index = [time for exploring the stranger mouse - time for exploring the empty cup] / total exploration time. Social novelty index = [time for exploring the novel stranger - time for exploring the old stranger] / total exploration time. Positive values indicate intact social and social novelty preferences. Animals that showed a bias for either chamber (stayed >7 min) in the habituation trial were excluded (n=1-2/group).

Social recognition

This test was used to assess social recognition memory. It included a learning trial (7 min) and a testing trial (7 min) with an inter-trial interval of 45 min. In the learning trial, a stranger was put underneath a cup on one side of the open field and an identical empty cup was placed on the other side. In the testing trial, another stranger was put underneath the previously empty cup. Physical contact around the cups by the subject's nose, head and forelimbs was defined as explorative behavior. Sociable index = [time for exploring the stranger mouse - time for exploring the empty cup] / total exploration time. Social novelty index = [time for exploring the novel stranger - time for exploring the old stranger] / total exploration time. Positive values indicate intact sociability and social memory [30]. Animals that did not explore all presented stimuli in either trial were excluded (n=1-2/group).

Object recognition

This test was used to assess object-based recognition memory. It included a learning trial and a testing trial with an inter-trial interval of 45 min. In the learning trial, two distinct objects were placed in the open

field and a subject freely explored them for 7 min. In the testing trial, one of the objects was replaced with a novel object and the subject explored them for 7 min. Object exploration was defined as physical contact with the objects by the head, nose, or forelimbs, but not other behaviors, such as climbing the objects or sitting next to them. To minimize individual differences, the index = [time for exploring the novel object - time for exploring the old object] / total exploration time was calculated. A positive value indicates intact object memory. Animals that did not explore all presented stimuli in either trial were excluded (n=1-2/group).

Histology, Immunohistochemistry, and Imaging

Mice were deeply anesthetized and perfused with ice-cold phosphate-buffered saline (PBS) followed by 4% paraformaldehyde. The brain was removed, immersed in 4% paraformaldehyde at 4°C overnight, transferred into 30% sucrose, and stored at 4°C until processed. The brain was sectioned into 40-50 µm-thick slices with a microtome (SM2010R, Leica Biosystems). The cerebellum was dissected out for examining distribution of fluorescent proteins with a Zeiss LSM 710 confocal microscope and therefore was not used for *c-Fos* immunostaining.

c-Fos

Same batch of c-kit$^{IRES\text{-}Cre}$ and their wild-type littermates that underwent behavioral testing were used for *c-Fos* staining (n=6/group). 90 min after the social recognition test, mice were sacrificed, and their brains were fixed. Brain sections were pretreated with 0.3% H_2O_2 for 10 min and incubated in a blocking solution (2% goat serum and 0.2% Triton X-100 in PBS) at 37°C for 30 min. Sections were then incubated with a rabbit anti-*c-Fos* antibody (1:4000, ab190289, Abcam, Cambridge, MA) at 4°C for 24-48 h. Sections were washed with 0.2% Triton X-100 and incubated with biotinylated anti-rabbit IgG (1:200, BA-1000, Vector Labs, Burlingame, CA) at room temperature for 2 h. After another rinse with 0.2% Triton X-100, sections were incubated in ABC Kit (Vector Labs) for 1 h. 3,3' diaminobenzidine chromogen was used for visualization. Sections were cover-slipped with a mounting medium (H-5000, Vector Labs) and imaged with a Leica DMi8 microscope under a 10x lens. 24 brain regions were identified based on a mouse brain atlas[86]. The number of *c-Fos*-positive cells in each region was

counted bilaterally across 2-4 serial sections with a 200 μm interval. Region of interest (ROI) was adjusted to the size of each brain region and the same ROI was applied to the same region between groups. The number of *c-Fos*-positive cells in each group was divided by the average value of the control group and presented as fold change. Experimenters who were blind to the design counted labeled cells with semi-automated analysis by ImageJ (NIH).

Neuronal tracing

Ai9 (RCL-tdT) mice (n=3) infused with AAV1-hSyn-Cre in the mDCN were used for anatomical studies. AAV1-hSyn-Cre has an anterograde transsynaptic property[64]. Via Cre-LoxP combination, neurons that receive input from the mDCN express tdTomato. 4-5 weeks after infusion, mice were sacrificed. Brain sections were collected in series with a 200 μm interval. Images were taken with a Zeiss LSM 710 confocal microscope. Location of somas, dendrites and axons of tdTomato-expressing neurons was identified based on a mouse brain atlas[86].

Interregional *c-Fos* Correlations and Graph Theoretical Analysis

Matrices of pairwise correlations were created by calculating Pearson coefficients (*r*) from the numbers of *c-Fos*-positive cells inter-regionally within each group. *r* was Fisher *Z* transformed. Statistics was conducted to compare average *r* between groups. Positive and negative *r* were indicated in red and indigo respectively in a gradient spectrum. Each node represented a brain region, and each connecting line represented Pearson's *r* between regions. Graph theoretical analysis was used to illustrate network properties for social recognition memory. The network was constructed with unweighted adjacency matrices for each group based on significant (uncorrected $p<0.05$) and positive ($r>0.6$) interregional correlations of *c-Fos* counts. Clusters were identified through enumeration of all potential community structures and optimization of the modularity. Degree (the number of edges that a node has) and betweenness (the number of shortest paths that pass through a node) were calculated to reveal the centrality of a node in the network. Within-community connectivity (*Z*-score, the extent of a node connected in its own community) and between-community connectivity (participation coefficient, the extent of a node connected to other communities) were calculated to reveal the modularity of the

network. Graph theoretical analysis was performed in MATLAB (R2015b) with Brain Connectivity Toolbox (https://sites.google.com/site/bctnet/). Calculation details were described previously[59,60].

Statistics

One-way or mixed two-way ANOVA with a between factor ("group") and a within factor ("object", "interval" or "trial") was applied to analyze data. Independent and paired *t*-tests were used when main effects were found. One sample *t*-test was used to compare the indices to 0 (chance level). Fisher's LSD was applied to *post hoc* tests when appropriate. Sample sizes were based on previous studies using similar experimental protocols[41,42,47]. For behavioral tests, *n* denoted the number of mice. For other analyses, *n* denoted the number of cells or samples from >3 mice/group. All statistics were two-tailed tests with significance set as $p<0.05$. Values were presented as mean ± standard error of the mean (SEM). Statistical details were summarized in **Supplementary Table 1**.

REFERENCES

1 Adolphs, R. The neurobiology of social cognition. *Curr Opin Neurobiol* **11**, 231-239, doi:10.1016/s0959-4388(00)00202-6 (2001).

2 Insel, T. R. & Fernald, R. D. How the brain processes social information: searching for the social brain. *Annu Rev Neurosci* **27**, 697-722, doi:10.1146/annurev.neuro.27.070203.144148 (2004).

3 Frith, C. D. & Frith, U. Mechanisms of social cognition. *Annu Rev Psychol* **63**, 287-313, doi:10.1146/annurev-psych-120710-100449 (2012).

4 Pelphrey, K., Adolphs, R. & Morris, J. P. Neuroanatomical substrates of social cognition dysfunction in autism. *Ment Retard Dev Disabil Res Rev* **10**, 259-271, doi:10.1002/mrdd.20040 (2004).

5 Couture, S. M., Penn, D. L. & Roberts, D. L. The functional significance of social cognition in schizophrenia: a review. *Schizophr Bull* **32 Suppl 1**, S44-63, doi:10.1093/schbul/sbl029 (2006).

6 Elamin, M., Pender, N., Hardiman, O. & Abrahams, S. Social cognition in neurodegenerative disorders: a systematic review. *J Neurol Neurosurg Psychiatry* **83**, 1071-1079, doi:10.1136/jnnp-2012-302817 (2012).

7 Cacciola, A. *et al.* The Known and Missing Links Between the Cerebellum, Basal Ganglia, and Cerebral Cortex. *Cerebellum* **16**, 753-755, doi:10.1007/s12311-017-0850-0 (2017).

8 Bostan, A. C. & Strick, P. L. The basal ganglia and the cerebellum: nodes in an integrated network. *Nat Rev Neurosci* **19**, 338-350, doi:10.1038/s41583-018-0002-7 (2018).

9 Stein, J. F. Role of the cerebellum in the visual guidance of movement. *Nature* **323**, 217-221, doi:10.1038/323217a0 (1986).

10 Jorntell, H., Bengtsson, F., Schonewille, M. & De Zeeuw, C. I. Cerebellar molecular layer interneurons - computational properties and roles in learning. *Trends Neurosci* **33**, 524-532, doi:10.1016/j.tins.2010.08.004 (2010).

11 Kim, J. & Augustine, G. J. Molecular Layer Interneurons: Key Elements of Cerebellar Network Computation and Behavior. *Neuroscience* **462**, 22-35, doi:10.1016/j.neuroscience.2020.10.008 (2021).

12 De Zeeuw, C. I. & Berrebi, A. S. Postsynaptic targets of Purkinje cell terminals in the cerebellar and vestibular nuclei of the rat. *Eur J Neurosci* **7**, 2322-2333, doi:10.1111/j.1460-9568.1995.tb00653.x (1995).

13 Schmahmann, J. D., Guell, X., Stoodley, C. J. & Halko, M. A. The Theory and Neuroscience of Cerebellar Cognition. *Annu Rev Neurosci* **42**, 337-364, doi:10.1146/annurev-neuro-070918-050258 (2019).

14 Strick, P. L., Dum, R. P. & Fiez, J. A. Cerebellum and nonmotor function. *Annu Rev Neurosci* **32**, 413-434, doi:10.1146/annurev.neuro.31.060407.125606 (2009).

15 Blatt, G. J., Oblak, A. L. & Schmahmann, J. D. in *Handbook of the Cerebellum and Cerebellar Disorders* (eds Mario Manto *et al.*) 479-496 (Springer Netherlands, 2013).

16 Wolpert, D. M., Miall, R. C. & Kawato, M. Internal models in the cerebellum. *Trends Cogn Sci* **2**, 338-347, doi:10.1016/s1364-6613(98)01221-2 (1998).

17 Ito, M. Control of mental activities by internal models in the cerebellum. *Nat Rev Neurosci* **9**, 304-313, doi:10.1038/nrn2332 (2008).

18 Sokolov, A. A., Miall, R. C. & Ivry, R. B. The Cerebellum: Adaptive Prediction for Movement and Cognition. *Trends Cogn Sci* **21**, 313-332, doi:10.1016/j.tics.2017.02.005 (2017).

19 Krienen, F. M. & Buckner, R. L. Segregated fronto-cerebellar circuits revealed by intrinsic functional connectivity. *Cereb Cortex* **19**, 2485-2497, doi:10.1093/cercor/bhp135 (2009).

20 Stoodley, C. J. & Schmahmann, J. D. Functional topography in the human cerebellum: a meta-analysis of neuroimaging studies. *Neuroimage* **44**, 489-501, doi:10.1016/j.neuroimage.2008.08.039 (2009).

21 Van Overwalle, F., Baetens, K., Marien, P. & Vandekerckhove, M. Social cognition and the cerebellum: a meta-analysis of over 350 fMRI studies. *Neuroimage* **86**, 554-572, doi:10.1016/j.neuroimage.2013.09.033 (2014).

22 Watson, T. C. *et al.* Anatomical and physiological foundations of cerebello-hippocampal interaction. *Elife* **8**, doi:10.7554/eLife.41896 (2019).

23 Zeidler, Z., Hoffmann, K. & Krook-Magnuson, E. HippoBellum: acute cerebellar modulation alters hippocampal dynamics and function. *J Neurosci* **40**, 6910-6926, doi:10.1523/JNEUROSCI.0763-20.2020 (2020).
24 Jackman, S. L. *et al.* Cerebellar Purkinje cell activity modulates aggressive behavior. *Elife* **9**, doi:10.7554/eLife.53229 (2020).
25 Stoodley, C. J. & Tsai, P. T. Adaptive Prediction for Social Contexts: The Cerebellar Contribution to Typical and Atypical Social Behaviors. *Annu Rev Neurosci* **44**, 475-493, doi:10.1146/annurev-neuro-100120-092143 (2021).
26 Kogan, J. H., Frankland, P. W. & Silva, A. J. Long-term memory underlying hippocampus-dependent social recognition in mice. *Hippocampus* **10**, 47-56, doi:10.1002/(SICI)1098-1063(2000)10:1<47::AID-HIPO5>3.0.CO;2-6 (2000).
27 Hitti, F. L. & Siegelbaum, S. A. The hippocampal CA2 region is essential for social memory. *Nature* **508**, 88-92, doi:10.1038/nature13028 (2014).
28 Okuyama, T., Kitamura, T., Roy, D. S., Itohara, S. & Tonegawa, S. Ventral CA1 neurons store social memory. *Science* **353**, 1536-1541, doi:10.1126/science.aaf7003 (2016).
29 Zinn, C. G. *et al.* Major neurotransmitter systems in dorsal hippocampus and basolateral amygdala control social recognition memory. *P Natl Acad Sci USA* **113**, E4914-E4919, doi:10.1073/pnas.1609883113 (2016).
30 Tanimizu, T. *et al.* Functional Connectivity of Multiple Brain Regions Required for the Consolidation of Social Recognition Memory. *J Neurosci* **37**, 4103-4116, doi:10.1523/JNEUROSCI.3451-16.2017 (2017).
31 Phillips, M. L., Robinson, H. A. & Pozzo-Miller, L. Ventral hippocampal projections to the medial prefrontal cortex regulate social memory. *Elife* **8**, doi:10.7554/eLife.44182 (2019).
32 Molenberghs, P., Cunnington, R. & Mattingley, J. B. Brain regions with mirror properties: a meta-analysis of 125 human fMRI studies. *Neurosci Biobehav Rev* **36**, 341-349, doi:10.1016/j.neubiorev.2011.07.004 (2012).
33 Van Overwalle, F., Ma, Q. & Heleven, E. The posterior crus II cerebellum is specialized for social mentalizing and emotional self-experiences: a meta-analysis. *Soc Cogn Affect Neurosci* **15**, 905-928, doi:10.1093/scan/nsaa124 (2020).
34 Gerwig, M., Kolb, F. P. & Timmann, D. The involvement of the human cerebellum in eyeblink conditioning. *Cerebellum* **6**, 38-57, doi:10.1080/14734220701225904 (2007).
35 Heiney, S. A., Kim, J., Augustine, G. J. & Medina, J. F. Precise control of movement kinematics by optogenetic inhibition of Purkinje cell activity. *J Neurosci* **34**, 2321-2330, doi:10.1523/JNEUROSCI.4547-13.2014 (2014).
36 ten Brinke, M. M. *et al.* Evolving Models of Pavlovian Conditioning: Cerebellar Cortical Dynamics in Awake Behaving Mice. *Cell Rep* **13**, 1977-1988, doi:10.1016/j.celrep.2015.10.057 (2015).
37 Boele, H. J. *et al.* Impact of parallel fiber to Purkinje cell long-term depression is unmasked in absence of inhibitory input. *Sci Adv* **4**, eaas9426, doi:10.1126/sciadv.aas9426 (2018).
38 Tsai, P. T. *et al.* Autistic-like behaviour and cerebellar dysfunction in Purkinje cell Tsc1 mutant mice. *Nature* **488**, 647-651, doi:10.1038/nature11310 (2012).
39 Cupolillo, D. *et al.* Autistic-Like Traits and Cerebellar Dysfunction in Purkinje Cell PTEN Knock-Out Mice. *Neuropsychopharmacology* **41**, 1457-1466, doi:10.1038/npp.2015.339 (2016).
40 Stoodley, C. J. *et al.* Altered cerebellar connectivity in autism and cerebellar-mediated rescue of autism-related behaviors in mice. *Nat Neurosci* **20**, 1744-1751, doi:10.1038/s41593-017-0004-1 (2017).
41 Chao, O. Y. *et al.* Targeting inhibitory cerebellar circuitry to alleviate behavioral deficits in a mouse model for studying idiopathic autism. *Neuropsychopharmacology* **45**, 1159-1170, doi:10.1038/s41386-020-0656-5 (2020).
42 Yang, Y. M. *et al.* Identification of a molecular locus for normalizing dysregulated GABA release from interneurons in the Fragile X brain. *Mol Psychiatry* **25**, 2017-2035, doi:10.1038/s41380-018-0240-0 (2020).

43 Bullitt, E. Expression of c-fos-like protein as a marker for neuronal activity following noxious stimulation in the rat. *J Comp Neurol* **296**, 517-530, doi:10.1002/cne.902960402 (1990).
44 Roth, B. L. DREADDs for Neuroscientists. *Neuron* **89**, 683-694, doi:10.1016/j.neuron.2016.01.040 (2016).
45 Amat, S. B. *et al.* Using c-kit to genetically target cerebellar molecular layer interneurons in adult mice. *PLoS One* **12**, e0179347, doi:10.1371/journal.pone.0179347 (2017).
46 Santamaria, F., Tripp, P. G. & Bower, J. M. Feedforward inhibition controls the spread of granule cell-induced Purkinje cell activity in the cerebellar cortex. *J Neurophysiol* **97**, 248-263, doi:10.1152/jn.01098.2005 (2007).
47 Chao, O. Y., Zhang, H., Pathak, S. S., Huston, J. P. & Yang, Y. M. Functional Convergence of Motor and Social Processes in Lobule IV/V of the Mouse Cerebellum. *Cerebellum*, doi:10.1007/s12311-021-01246-7 (2021).
48 Badura, A. *et al.* Normal cognitive and social development require posterior cerebellar activity. *Elife* **7**, doi:10.7554/eLife.36401 (2018).
49 Silverman, J. L., Yang, M., Lord, C. & Crawley, J. N. Behavioural phenotyping assays for mouse models of autism. *Nat Rev Neurosci* **11**, 490-502, doi:10.1038/nrn2851 (2010).
50 Chao, O. Y., de Souza Silva, M. A., Yang, Y. M. & Huston, J. P. The medial prefrontal cortex - hippocampus circuit that integrates information of object, place and time to construct episodic memory in rodents: Behavioral, anatomical and neurochemical properties. *Neurosci Biobehav Rev* **113**, 373-407, doi:10.1016/j.neubiorev.2020.04.007 (2020).
51 Josselyn, S. A. & Tonegawa, S. Memory engrams: Recalling the past and imagining the future. *Science* **367**, doi:10.1126/science.aaw4325 (2020).
52 Boyden, E. S., Zhang, F., Bamberg, E., Nagel, G. & Deisseroth, K. Millisecond-timescale, genetically targeted optical control of neural activity. *Nat Neurosci* **8**, 1263-1268, doi:10.1038/nn1525 (2005).
53 Kim, J. *et al.* Optogenetic mapping of cerebellar inhibitory circuitry reveals spatially biased coordination of interneurons via electrical synapses. *Cell Rep* **7**, 1601-1613, doi:10.1016/j.celrep.2014.04.047 (2014).
54 Herweg, N. A., Solomon, E. A. & Kahana, M. J. Theta Oscillations in Human Memory. *Trends Cogn Sci* **24**, 208-227, doi:10.1016/j.tics.2019.12.006 (2020).
55 Dave, S., VanHaerents, S. & Voss, J. L. Cerebellar Theta and Beta Noninvasive Stimulation Rhythms Differentially Influence Episodic Memory versus Semantic Prediction. *J Neurosci* **40**, 7300-7310, doi:10.1523/JNEUROSCI.0595-20.2020 (2020).
56 Hughes, P., Lawlor, P. & Dragunow, M. Basal expression of Fos, Fos-related, Jun, and Krox 24 proteins in rat hippocampus. *Brain Res Mol Brain Res* **13**, 355-357, doi:10.1016/0169-328x(92)90219-2 (1992).
57 Chaudhuri, A., Zangenehpour, S., Rahbar-Dehgan, F. & Ye, F. Molecular maps of neural activity and quiescence. *Acta Neurobiol Exp (Wars)* **60**, 403-410 (2000).
58 Aminoff, E. M., Kveraga, K. & Bar, M. The role of the parahippocampal cortex in cognition. *Trends Cogn Sci* **17**, 379-390, doi:10.1016/j.tics.2013.06.009 (2013).
59 Newman, M. E. & Girvan, M. Finding and evaluating community structure in networks. *Phys Rev E Stat Nonlin Soft Matter Phys* **69**, 026113, doi:10.1103/PhysRevE.69.026113 (2004).
60 Guimera, R. & Amaral, L. A. Cartography of complex networks: modules and universal roles. *J Stat Mech* **2005**, nihpa35573, doi:10.1088/1742-5468/2005/02/P02001 (2005).
61 Hermans, E. J. *et al.* How the amygdala affects emotional memory by altering brain network properties. *Neurobiol Learn Mem* **112**, 2-16, doi:10.1016/j.nlm.2014.02.005 (2014).
62 McEwen, B. S., Nasca, C. & Gray, J. D. Stress Effects on Neuronal Structure: Hippocampus, Amygdala, and Prefrontal Cortex. *Neuropsychopharmacology* **41**, 3-23, doi:10.1038/npp.2015.171 (2016).
63 Madisen, L. *et al.* A robust and high-throughput Cre reporting and characterization system for the whole mouse brain. *Nat Neurosci* **13**, 133-140, doi:10.1038/nn.2467 (2010).
64 Zingg, B. *et al.* AAV-mediated anterograde transsynaptic tagging: Mapping corticocollicular input-defined neural pathways for defense behaviors. *Neuron* **93**, 33-47, doi:10.1016/j.neuron.2016.11.045 (2017).
65 Carta, I., Chen, C. H., Schott, A. L., Dorizan, S. & Khodakhah, K. Cerebellar modulation of the reward circuitry and social behavior. *Science* **363**, doi:10.1126/science.aav0581 (2019).

66 Kelly, E. *et al.* Regulation of autism-relevant behaviors by cerebellar-prefrontal cortical circuits. *Nat Neurosci* **23**, 1102-1110, doi:10.1038/s41593-020-0665-z (2020).
67 Fujita, H., Kodama, T. & du Lac, S. Modular output circuits of the fastigial nucleus for diverse motor and nonmotor functions of the cerebellar vermis. *Elife* **9**, doi:10.7554/eLife.58613 (2020).
68 Pisano, T. J. *et al.* Homologous organization of cerebellar pathways to sensory, motor, and associative forebrain. *Cell Rep* **36**, 109721, doi:10.1016/j.celrep.2021.109721 (2021).
69 Dietrichs, E. & Haines, D. E. Interconnections between hypothalamus and cerebellum. *Anat Embryol (Berl)* **179**, 207-220, doi:10.1007/bf00326585 (1989).
70 Zhu, J. N., Yung, W. H., Kwok-Chong Chow, B., Chan, Y. S. & Wang, J. J. The cerebellar-hypothalamic circuits: potential pathways underlying cerebellar involvement in somatic-visceral integration. *Brain Res Rev* **52**, 93-106, doi:10.1016/j.brainresrev.2006.01.003 (2006).
71 Low, A. Y. T. *et al.* Reverse-translational identification of a cerebellar satiation network. *Nature* **600**, 269-273, doi:10.1038/s41586-021-04143-5 (2021).
72 Sigurdsson, T. & Duvarci, S. Hippocampal-Prefrontal Interactions in Cognition, Behavior and Psychiatric Disease. *Front Syst Neurosci* **9**, 190, doi:10.3389/fnsys.2015.00190 (2015).
73 Janak, P. H. & Tye, K. M. From circuits to behaviour in the amygdala. *Nature* **517**, 284-292, doi:10.1038/nature14188 (2015).
74 Wulff, P. *et al.* Synaptic inhibition of Purkinje cells mediates consolidation of vestibulo-cerebellar motor learning. *Nat Neurosci* **12**, 1042-1049, doi:10.1038/nn.2348 (2009).
75 Rowan, M. J. M. *et al.* Graded Control of Climbing-Fiber-Mediated Plasticity and Learning by Inhibition in the Cerebellum. *Neuron* **99**, 999-1015 e1016, doi:10.1016/j.neuron.2018.07.024 (2018).
76 Schmahmann, J. D. & Sherman, J. C. The cerebellar cognitive affective syndrome. *Brain* **121 (Pt 4)**, 561-579, doi:10.1093/brain/121.4.561 (1998).
77 Lefort, J. M. *et al.* Impaired cerebellar Purkinje cell potentiation generates unstable spatial map orientation and inaccurate navigation. *Nat Commun* **10**, 2251, doi:10.1038/s41467-019-09958-5 (2019).
78 Deverett, B., Koay, S. A., Oostland, M. & Wang, S. S. Cerebellar involvement in an evidence-accumulation decision-making task. *Elife* **7**, doi:10.7554/eLife.36781 (2018).
79 Deverett, B., Kislin, M., Tank, D. W. & Wang, S. S. Cerebellar disruption impairs working memory during evidence accumulation. *Nat Commun* **10**, 3128, doi:10.1038/s41467-019-11050-x (2019).
80 Ma, M. *et al.* Molecular layer interneurons in the cerebellum encode for valence in associative learning. *Nat Commun* **11**, 4217, doi:10.1038/s41467-020-18034-2 (2020).
81 Krach, S., Paulus, F. M., Bodden, M. & Kircher, T. The rewarding nature of social interactions. *Front Behav Neurosci* **4**, 22, doi:10.3389/fnbeh.2010.00022 (2010).
82 Liu, Y., McAfee, S., Sillitoe, R. & Heck, D. Cerebellar modulation of prefrontal-hippocampal gamma coherence during spatial working memory decisions. *bioRxiv* (2020).
83 Zeineh, M. M., Engel, S. A., Thompson, P. M. & Bookheimer, S. Y. Dynamics of the hippocampus during encoding and retrieval of face-name pairs. *Science* **299**, 577-580, doi:10.1126/science.1077775 (2003).
84 Eldridge, L. L., Engel, S. A., Zeineh, M. M., Bookheimer, S. Y. & Knowlton, B. J. A dissociation of encoding and retrieval processes in the human hippocampus. *J Neurosci* **25**, 3280-3286, doi:10.1523/JNEUROSCI.3420-04.2005 (2005).
85 Eichenbaum, H., Yonelinas, A. P. & Ranganath, C. The medial temporal lobe and recognition memory. *Annu Rev Neurosci* **30**, 123-152, doi:10.1146/annurev.neuro.30.051606.094328 (2007).
86 Franklin, K. B. J. & Paxinos, G. *The mouse brain in stereotaxic coordinates, compact third edition*. (Elsevier, 2008).

FIGURE LEGENDS

Fig 1. Chemogenetic excitation of MLIs in cerebellar lobules IV-VII disrupted social, but not object, recognition memory. (**a**) Design to specifically target MLIs by infusion of AAV8-hSyn-DIO-hM3Dq-mCherry (hM3Dq) into the anterior (lobule IV/V) or posterior (lobule VI/VII) vermis of a c-kit$^{IRES\text{-}Cre}$ mouse. (**b**) Examples of AAV-mediated expression of hM3Dq in MLIs (right) in lobule IV/V (left) or VI/VII (middle). ML, molecular layer; PL, Purkinje layer; GL, granular layer. (**c**) Cell-attached patch-clamp recordings of APs from MLIs (basket cells) expressing hM3Dq (top) or not (bottom) before and after CNO application (10 μM). (**d**) Effects of CNO on firing frequency of hM3Dq-containing (n=5) and hM3Dq-lacking (n=6) MLIs. (**e**) A three-chamber social test included a sociability and a social novelty trial with no time delay in between (left). All groups showed intact sociability (explored the stranger more than the cup) and intact social novelty (explored the novel stranger more than the old one), except for vermis VI/VII group (right). (**f**) A social recognition test included a learning and a testing trial with an inter-trial interval of 45 min (left). All groups displayed intact sociability, but perturbation of lobule IV/V or VI/VII impaired animals' social recognition (explored the novel and the old strangers indiscriminately) (right). (**g**) An object recognition test included a learning and a testing trial with an inter-trial interval of 45 min (left). All groups had intact object recognition (explored the novel object more than the old one) (right). Littermates without Cre recombinase served as controls. CNO (1 mg/kg) was given 30-40 min before each test. In the sociability trial of three-chamber tests and in the learning trial of social recognition tests: index= [time for exploring the stranger - time for exploring the cup] / total exploration time. In the social novelty trial of three-chamber tests and in the testing trials of social and object recognition tests: index= [time for exploring the novel one - time for exploring the old one] / total exploration time. Positive values of indices suggest intact performance. *p<0.05, paired t-test. #p<0.05, one-sample t-test compared to 0. *ns*, not significant. n=7-9 mice/group for behavior tests.

Fig 2. Optogenetic stimulation of MLIs in cerebellar lobules IV-VII in the retrieval, but not the encoding, phase impaired social recognition memory. (**a**) Sagittal cerebellar slice from a nNOS-ChR2 mouse (left). Co-labeling of PCs with an anti-Calbindin antibody showed selective expression of

ChR2 (visualized with YFP) in the soma and processes of MLIs (right). ML, molecular layer; PL, Purkinje layer; GL, granular layer; ChR2, channelrhodopsin-2; YFP, yellow fluorescent protein. (**b**) APs recorded from MLIs (middle) and PCs (bottom) of a nNOS-ChR2 mouse in response to light stimulation (25 ms, 8 Hz, top). (**c**, **d**) Light stimulation increased frequency of APs elicited from MLIs (n=7; **c**) but decreased it from PCs and increased coefficient of variation (CV) of inter-AP intervals for PCs (n=9; **d**). (**e**, **f**) In a social recognition test, light delivery (25 ms, 8 Hz, 10 s pause every 50 s) in the learning trial did not affect animals' social approach (explored the stranger more than the cup) or social recognition (explored the novel stranger more than the old one) (**e**). Same light delivery in the testing trial impaired animals' social recognition (explored the novel and the old strangers equally) without affecting their social preference (explored the stranger more than the cup) (**f**). (**g**) Same light delivery in the testing trial of an object recognition test had no effect on animals' object recognition (explored the novel object more than the old one). Littermates (not expressing ChR2) served as controls. In the learning trial of social recognition tests: index= [time for exploring the stranger - time for exploring the cup] / total exploration time. In the testing trial of social and object recognition tests: index= [time for exploring the novel one - time for exploring the old one] / total exploration time. Positive values of indices suggest intact performance. *p<0.05, paired t-test. #p<0.05, one-sample t-test compared to 0. *ns*, not significant. n=7-9 mice/group for behavior tests.

Fig 3. Altered *c-Fos* expression by chemogenetic excitation of MLIs in cerebellar lobules IV-VII following the social recognition test. (**a**) Design of *c-Fos* imaging after the social recognition test. (**b**, **c**) Examples of *c-Fos* staining (black dots) in the PL (**b**), BLA and CeA (**c**) subregions. Fold change, defined as the number of *c-Fos*-positive cells in each group divided by the average value of the control group, was summarized for all subregions in the medial prefrontal cortex and amygdala. *p<0.05, Fisher's LSD test. *ns*, not significant. n=6 mice/group. Acg, anterior cingulate cortex (rostral); PL, prelimbic cortex; IL, infralimbic cortex; CeA, central nucleus of amygdala; BLA, basolateral amygdala; BMP, basomedial amygdala.

Fig 4. Chemogenetic excitation of MLIs in cerebellar lobules IV-VII reduced interregional connectivity activated by social recognition. (**a**) Matrices of interregional correlations derived from *c-Fos*-positive cells. Colors indicate the scale of Pearson coefficients (*r*) from 1 (red) to -1 (indigo). (**b**) Network graphs of significantly positive ($r>0.6$, red lines) or negative ($r<-0.6$, indigo lines) correlations. (**c**) Pie charts of relative proportions of positive (red) and negative (indigo) correlations. (**d**) Summary of average *r* in calculation of all interregional correlation coefficients. (**e**-**h**) Matrices of interregional correlations for subregions in the medial prefrontal cortex (**e**), anterior cingulate cortex (**f**), hippocampus (**g**), and amygdala (**h**). *$p<0.05$, Fisher's LSD test. *ns*, not significant. n=6 mice/group. Acg, anterior cingulate cortex (rostral); PL, prelimbic cortex; IL, infralimbic cortex; OFC, orbitofrontal cortex; ACC, anterior cingulate cortex; M1, primary motor cortex; dSTR, dorsal striatum; NAc, nucleus accumbens; RSD, dorsal retrosplenial cortex; RSG, retrosplenial granular area; PtA, parietal association cortex; TeA, temporal association areas; Ect, ectorhinal cortex; PRh, perirhinal cortex; lEnt, lateral entorhinal cortex; CA1, hippocampus CA1; CA2/3, hippocampus CA2/3; DG, dentate gyrus; CeA, central nucleus of amygdala; BLA, basolateral amygdala; BMP, basomedial amygdala; vTH, ventral thalamus; mHA, medial hypothalamus; VTA, ventral tegmental area.

Fig 5. Chemogenetic excitation of MLIs in cerebellar lobules IV-VII disrupted modular structure of social recognition network. (**a**-**c**) Rankings of normalized degree (left), betweenness (middle), within-community *Z*-scores and participation coefficients (right) of brain regions for control (**a**), vermis IV/V (**b**), and vermis VI/VII (**c**) groups. (**d**-**f**) Hubs revealed by graph theoretical analysis of neural networks activated during social recognition in all groups. Hubs were defined with modularity maximization, based on within-community *Z*-score and participation coefficient of each region. Distinct communities were color coded. Size of nodes (brain regions) was proportional to their degree. Note that participation coefficients for vermis IV/V and VI/VII groups were zero and thus they did not form >1 module. ACC, anterior cingulate cortex; Acg, anterior cingulate cortex (rostral); BLA, basolateral amygdala; BMP, basomedial amygdala; CA1, hippocampus CA1; CA2/3, hippocampus CA2/3; CeA, central nucleus of amygdala; DG, dentate gyrus; dSTR, dorsal striatum; Ect, ectorhinal cortex; IL,

infralimbic cortex; lEnt, lateral entorhinal cortex; M1, primary motor cortex; mHA, medial hypothalamus; NAc, nucleus accumbens; OFC, orbitofrontal cortex; PL, prelimbic cortex; PRh, perirhinal cortex; PtA, parietal association cortex; RSD, dorsal retrosplenial cortex; RSG, retrosplenial granular area; TeA, temporal association areas; VTA, ventral tegmental area; vTH, ventral thalamus.

Fig 6. Transsynaptic tracing of cerebellar-cortical circuits. (**a**) Schematic of anterograde tracing by injecting AAV1-hSyn-Cre into the mDCN of a Ai9 mouse that has a LoxP site. Via Cre-LoxP recombination, transduced neurons in the mDCN express tdTomato and project axons to a 1st-order downstream nucleus. As the virus has a transsynaptic property, it further transduces neurons in the 1st-order station, which send axons to a 2nd-order nucleus. (**b**) Neurons in the mDCN (FN and IN) were primarily targeted (n=3 mice). FN, fastigial nucleus; IN, interposed nucleus; DN, dentate nucleus; AP, anterior-posterior axis. Occasionally, the virus retrogradely transfected PCs in the cerebellar cortex. (**c**, **d**) Examples of tdTomato labeling of somas, dendrites, and axons in 1st- and 2nd-order nuclei. vTH, ventral thalamus; VTA, ventral tegmental area; VL, ventrolateral thalamus; VM, ventromedial thalamus; AM, anteromedial thalamus; MD, mediodorsal thalamus; VPM, ventral posteromedial thalamus; PF, parafascicular thalamus; CL, centrolateral thalamus; dSTR, dorsal striatum; BLA, basolateral amygdala; M1, primary motor cortex; PtA, parietal association cortex; Ect, ectorhinal area; Acg, anterior cingulate cortex (rostral); PL, prelimbic cortex; IL, infralimbic cortex; ACC, anterior cingulate cortex.

Supplementary Fig 1. Chemogenetic excitation of MLIs in cerebellar lobules IV-VII did not affect anxiety levels, locomotor activity, motor coordination or free social interaction. (**a**-**d**) No differences were found between control, vermis IV/V, and vermis VI/VII groups in behavioral parameters obtained from elevated plus maze (**a**), open field (**b**), rotarod (**c**) and reciprocal social interaction (**d**) tests. One-way or two-way ANOVA was used for group comparisons. n=7-9 mice/group.

Supplementary Fig 2. Effects of chemogenetic excitation of MLIs in cerebellar lobules IV-VII on *c-Fos* expression in different brain regions after the social recognition test. Fold change, defined

as the number of *c-Fos*-positive cells in each group divided by the average value of the control group, was summarized for all regions. *p<0.05, Fisher's LSD test. n=6 mice/group. OFC, orbitofrontal cortex; ACC, anterior cingulate cortex; M1, primary motor cortex; dSTR, dorsal striatum; NAc, nucleus accumbens; RSD, dorsal retrosplenial cortex; RSG, retrosplenial granular area; PtA, parietal association cortex; TeA, temporal association areas; Ect, ectorhinal cortex; PRh, perirhinal cortex; lEnt, lateral entorhinal cortex; CA1, hippocampus CA1; CA2/3, hippocampus CA2/3; DG, dentate gyrus; vTH, ventral thalamus; mHA, medial hypothalamus; VTA, ventral tegmental area.

Figure 1

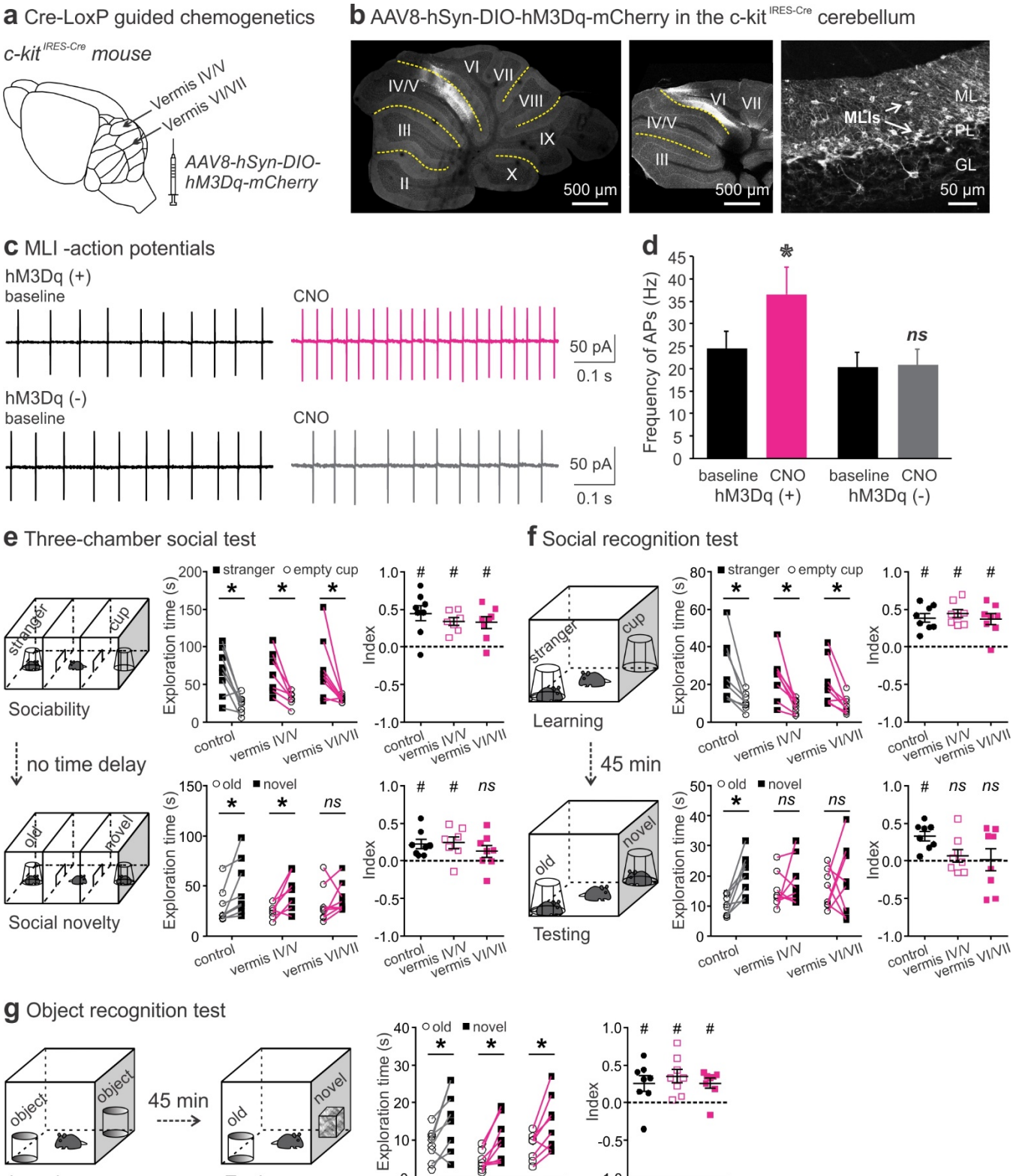
a Cre-LoxP guided chemogenetics
c-kit IRES-Cre mouse
Vermis IV/V
Vermis VI/VII
AAV8-hSyn-DIO-hM3Dq-mCherry
b AAV8-hSyn-DIO-hM3Dq-mCherry in the c-kit IRES-Cre cerebellum
VI
VII
IV/V
VIII
III
IX
II
X
500 µm
MLIs
ML
PL
GL
50 µm
c MLI -action potentials
hM3Dq (+)
baseline
CNO
50 pA
0.1 s
hM3Dq (-)
d
Frequency of APs (Hz)
ns
baseline CNO baseline CNO
hM3Dq (+) hM3Dq (-)
e Three-chamber social test
stranger
cup
Sociability
no time delay
old
novel
Social novelty
stranger
empty cup
Exploration time (s)
Index
control
vermis IV/V
vermis VI/VII
f Social recognition test
Learning
45 min
Testing
g Object recognition test
object
Learning
45 min
Testing

Figure 2

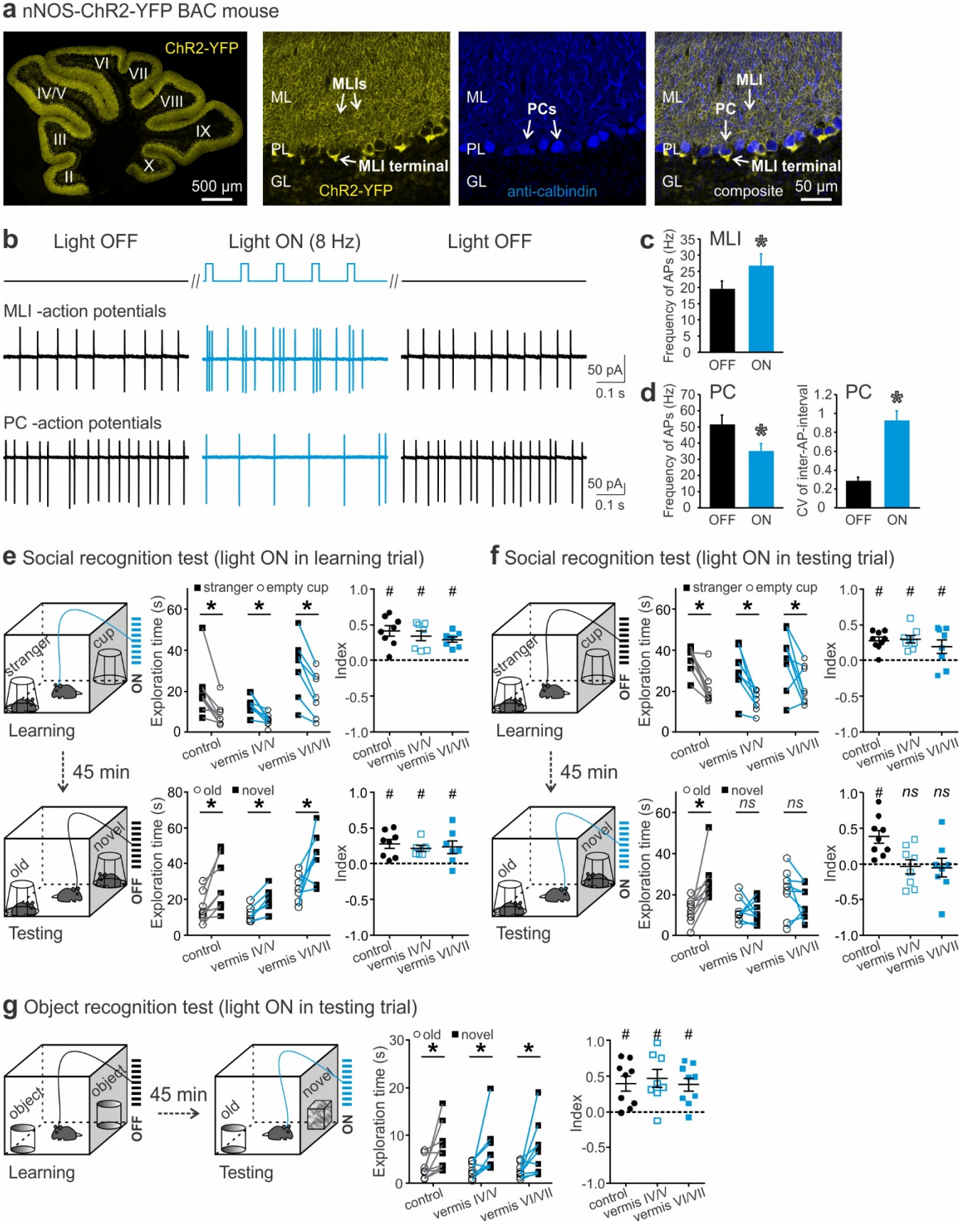
a nNOS-ChR2-YFP BAC mouse
ChR2-YFP
VI
VII
IV/V
VIII
IX
III
X
II
500 µm
MLIs
ML
PL
GL
MLI terminal
ChR2-YFP
PCs
anti-calbindin
MLI
PC
composite
50 µm
b
Light OFF
Light ON (8 Hz)
Light OFF
MLI -action potentials
PC -action potentials
50 pA
0.1 s
c
MLI
Frequency of APs (Hz)
OFF
ON
d
PC
CV of inter-AP-interval
e Social recognition test (light ON in learning trial)
f Social recognition test (light ON in testing trial)
stranger
empty cup
cup
Learning
45 min
old
novel
Testing
Exploration time (s)
Index
control
vermis IV/V
vermis VI/VII
ns
g Object recognition test (light ON in testing trial)
object

Figure 3

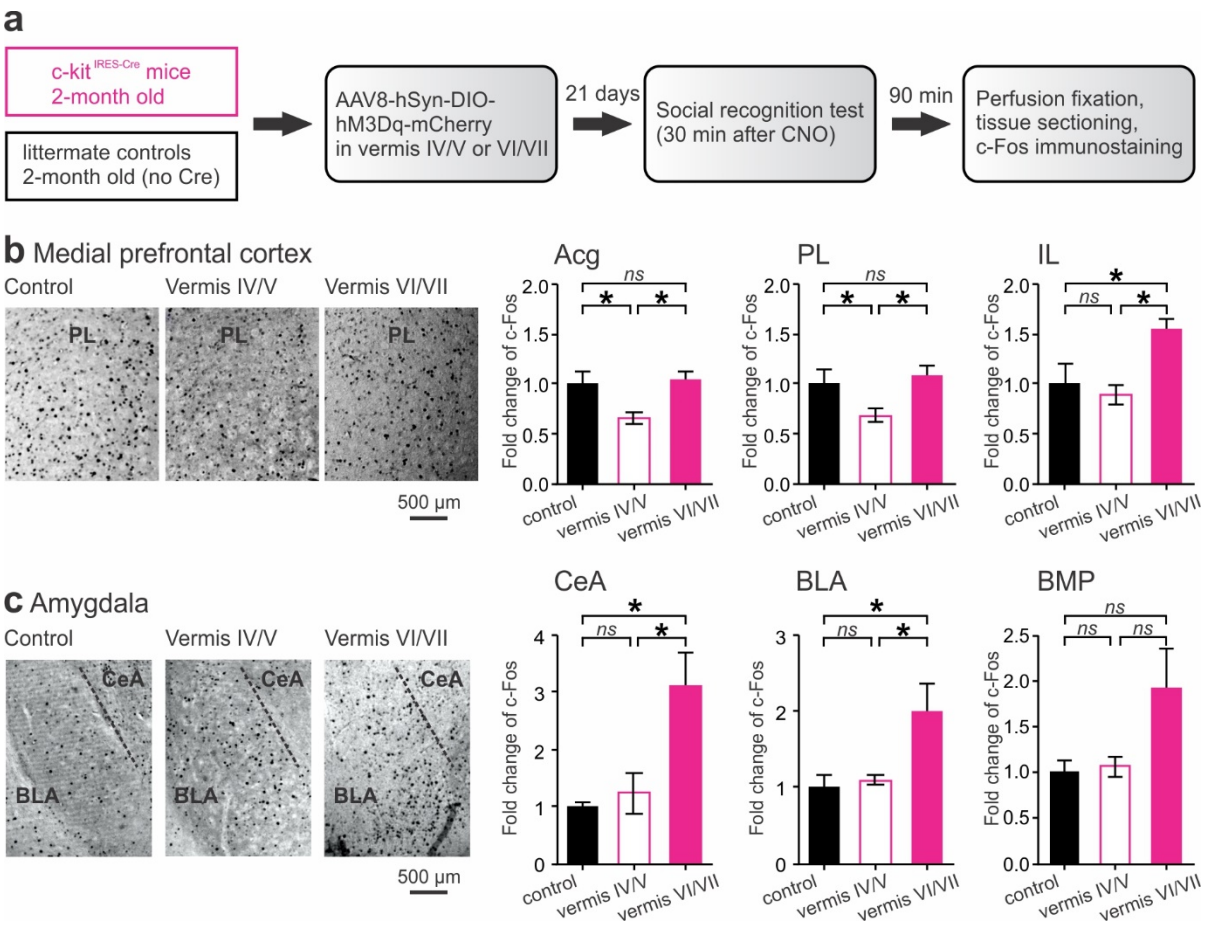
a
c-kit IRES-Cre mice
2-month old
littermate controls
2-month old (no Cre)
AAV8-hSyn-DIO-
hM3Dq-mCherry
in vermis IV/V or VI/VII
21 days
Social recognition test
(30 min after CNO)
90 min
Perfusion fixation,
tissue sectioning,
c-Fos immunostaining
b Medial prefrontal cortex
Control
Vermis IV/V
Vermis VI/VII
PL
500 µm
Acg
PL
IL
Fold change of c-Fos
control
vermis IV/V
vermis VI/VII
ns
c Amygdala
CeA
BLA
BMP

Figure 4

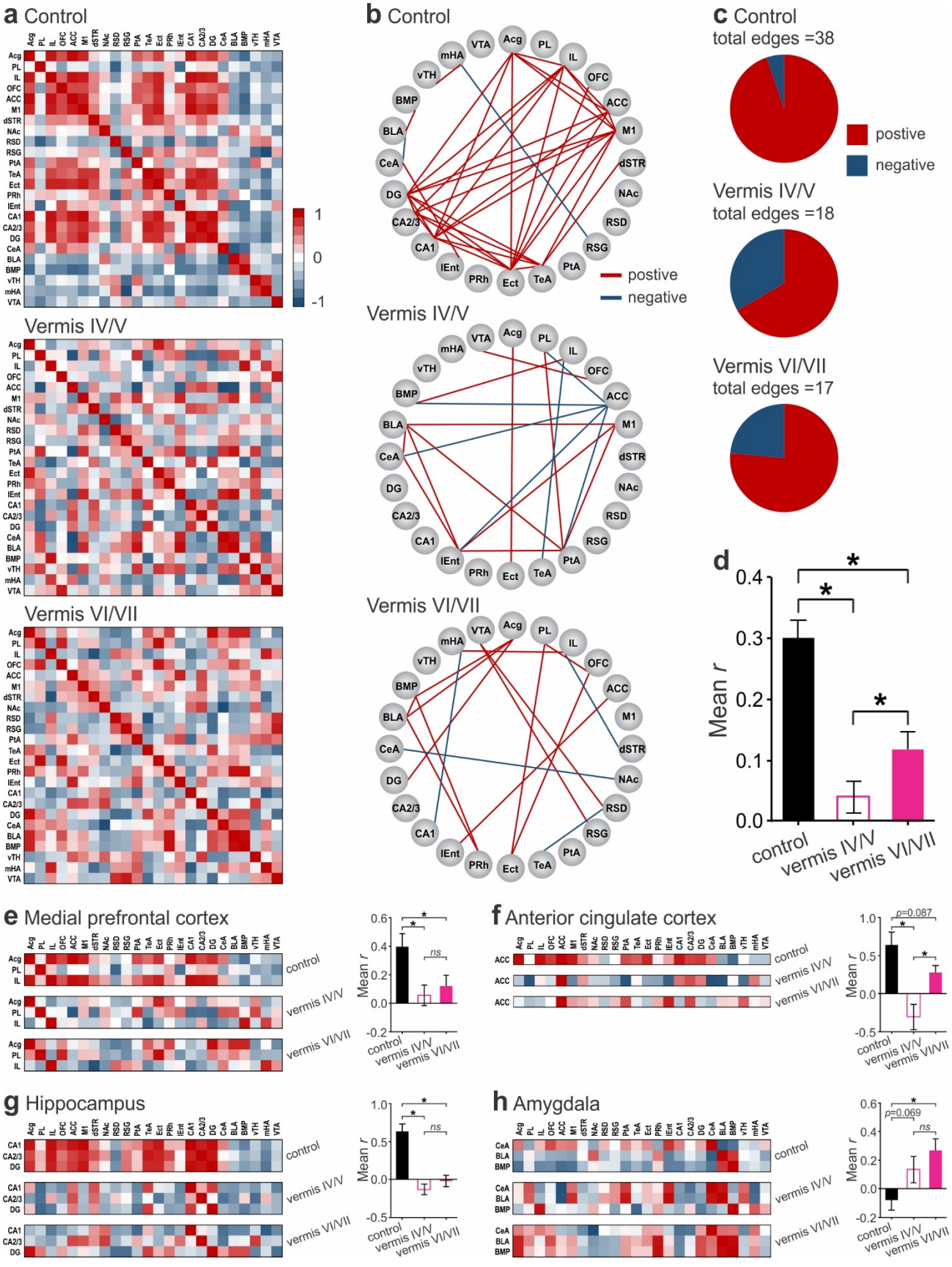
a Control
Vermis IV/V
Vermis VI/VII
1
0
-1
b Control
postive
negative
Vermis IV/V
Vermis VI/VII
c Control
total edges =38
postive
negative
Vermis IV/V
total edges =18
Vermis VI/VII
total edges =17
d
Mean r
control
vermis IV/V
vermis VI/VII
e Medial prefrontal cortex
f Anterior cingulate cortex
p=0.087
g Hippocampus
h Amygdala
p=0.069
ns

Figure 5

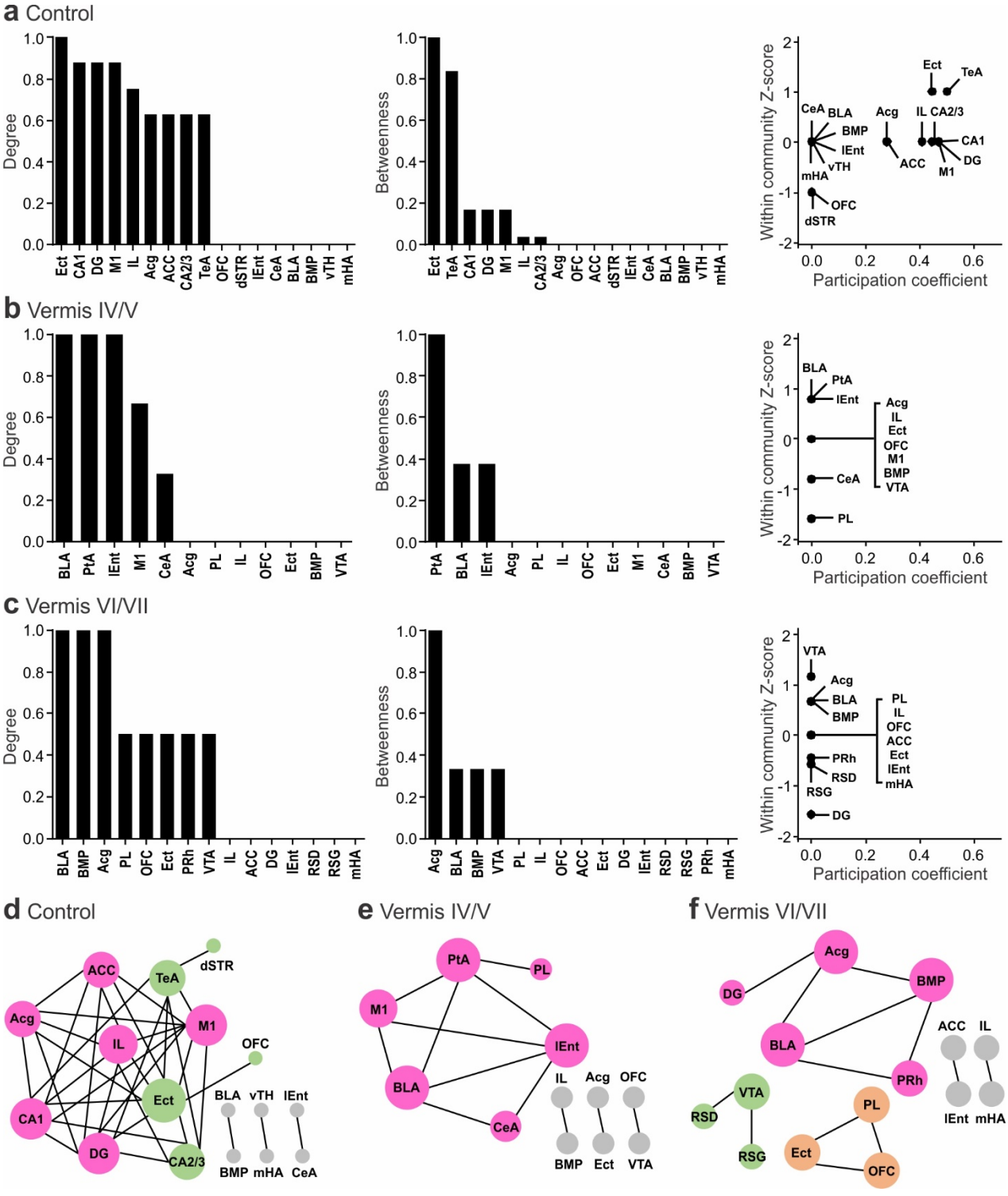
a Control
Degree
Betweenness
Within community Z-score
Participation coefficient
b Vermis IV/V
c Vermis VI/VII
d Control
e Vermis IV/V
f Vermis VI/VII

Figure 6

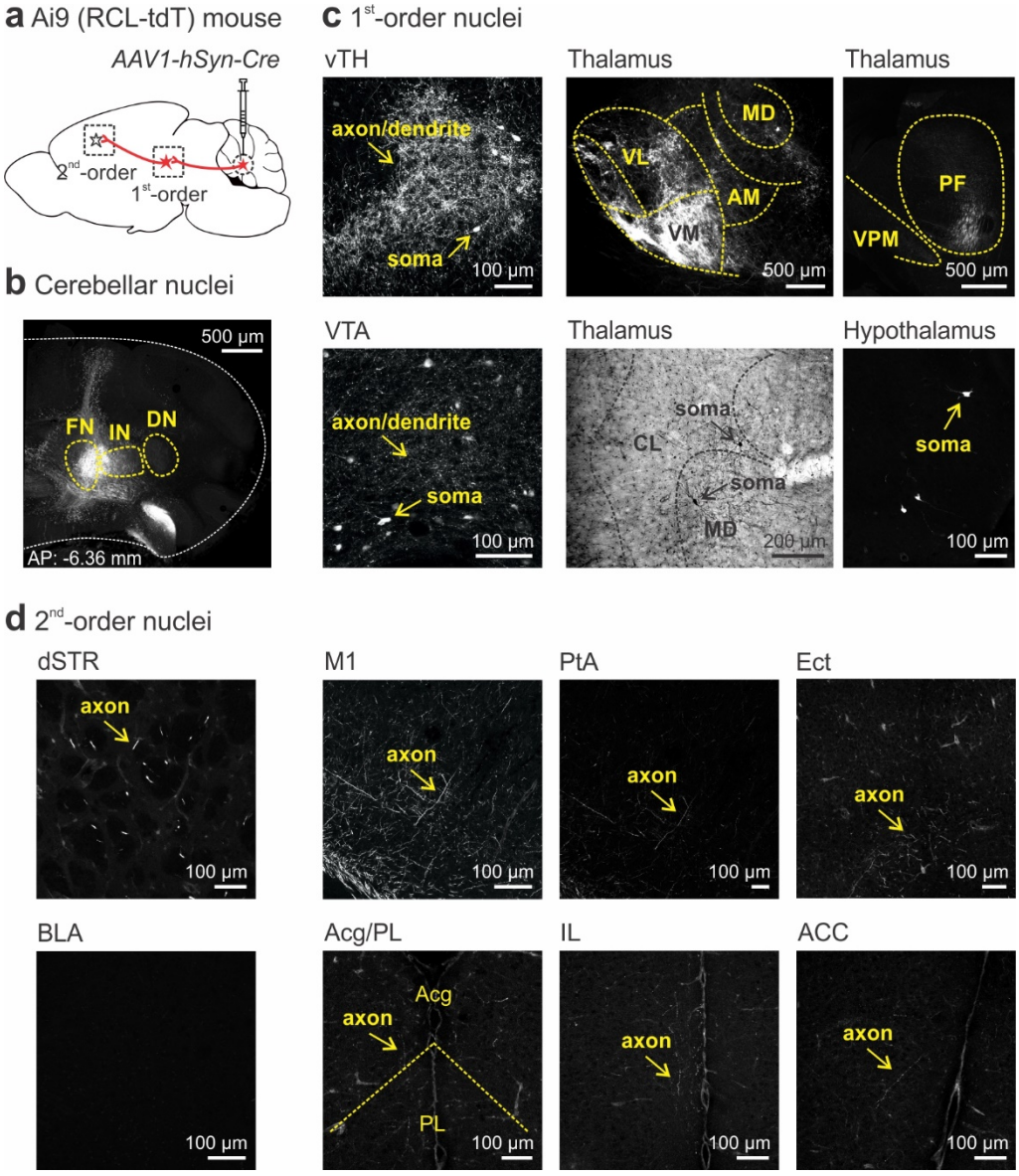
a Ai9 (RCL-tdT) mouse
AAV1-hSyn-Cre
2nd-order
1st-order
b Cerebellar nuclei
500 μm
FN
IN
DN
AP: -6.36 mm
c 1st-order nuclei
vTH
axon/dendrite
soma
100 μm
Thalamus
MD
VL
AM
VM
500 μm
Thalamus
PF
VPM
500 μm
VTA
axon/dendrite
soma
100 μm
Thalamus
soma
CL
soma
MD
200 μm
Hypothalamus
soma
100 μm
d 2nd-order nuclei
dSTR
axon
100 μm
M1
axon
100 μm
PtA
axon
100 μm
Ect
axon
100 μm
BLA
100 μm
Acg/PL
Acg
axon
PL
100 μm
IL
axon
100 μm
ACC
axon
100 μm

Supplementary Figure 1

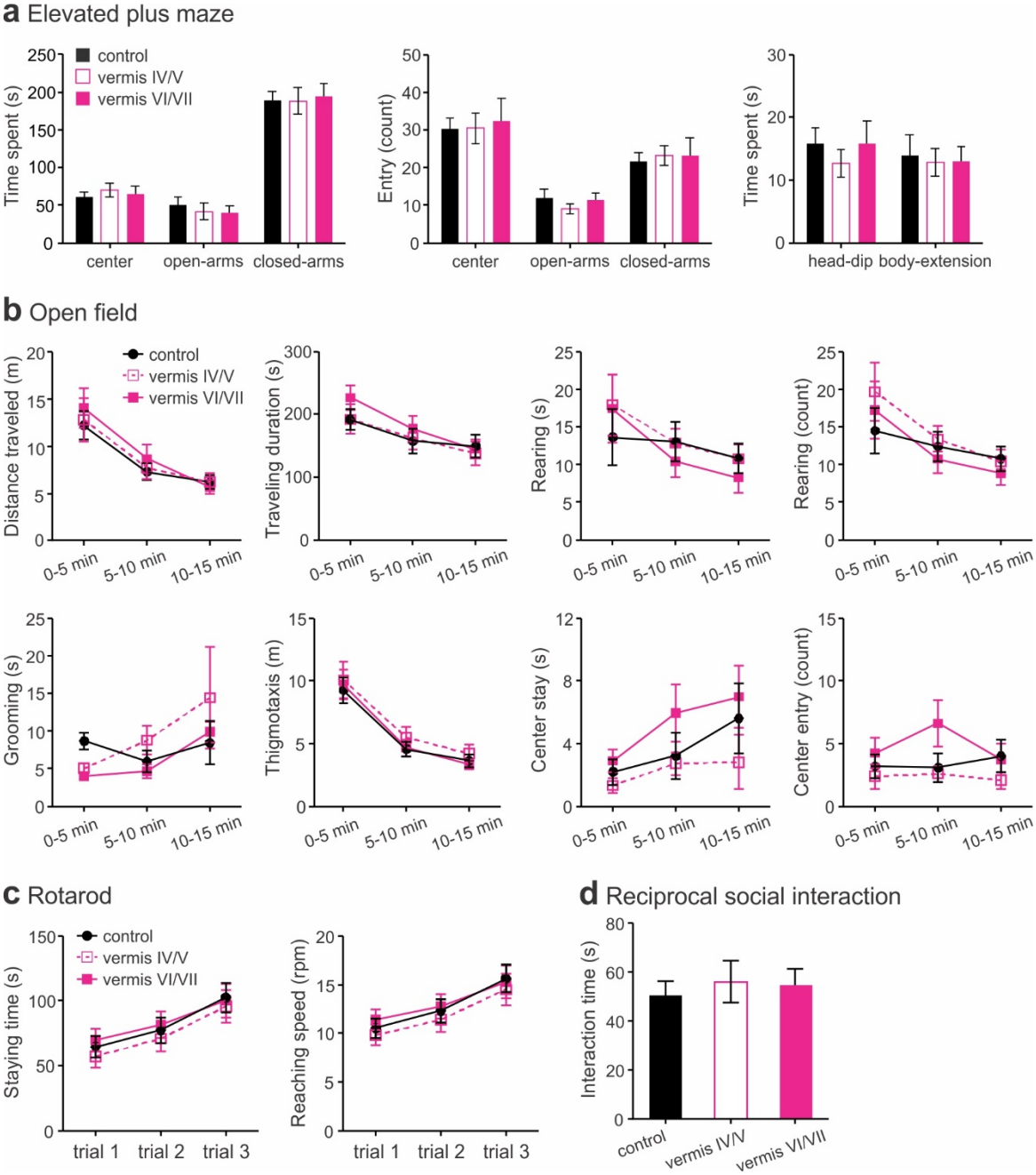

Supplementary Figure 2

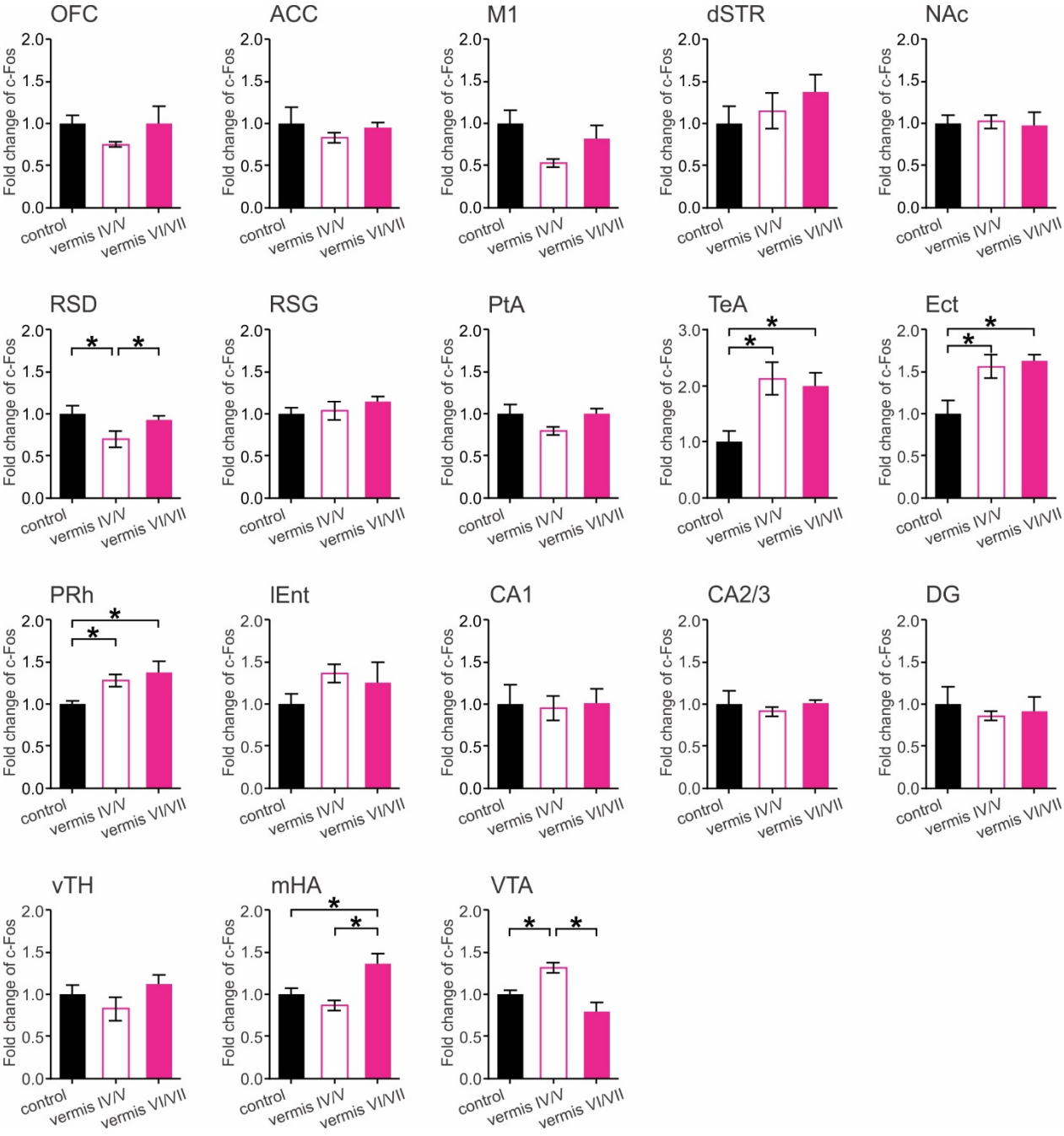

Supplementary Table 1. A list of statistical analyses.

Chemogenetic manipulation – electrophysiology	
One-way ANOVA hM3Dq (+) vs. hM3Dq (-) BCs	AP frequency at baseline: "group" effect $F_{1,9}$=0.722, p>0.05
Paired *t*-test within each group baseline vs. CNO	hM3Dq (+) BCs: t_4=-4.488, ***p*=0.011** hM3Dq (-) BCs: t_5=-0.484, p>0.05
Chemogenetic manipulation – behavioral testing	
Elevated plus maze	
One-way ANOVA	center time: "group" effect $F_{2,25}$=0.3, p>0.05 open-arms time: "group" effect $F_{2,25}$=0.262, p>0.05 closed-arms time: "group" effect $F_{2,25}$=0.053, p>0.05 center entry: "group" effect $F_{2,25}$=0.072, p>0.05 open-arms entry: "group" effect $F_{2,25}$=0.74, p>0.05 closed-arms entry: "group" effect $F_{2,25}$=0.091, p>0.05 head-dip time: "group" effect $F_{2,25}$=0.478, p>0.05 body-extension time: "group" effect $F_{2,25}$=0.056, p>0.05 distance travelled: "group" effect $F_{2,25}$=0.443, p>0.05
Open field	
Mixed two-way ANOVA (distance traveled)	"group" effect $F_{2,25}$=0.152, p>0.05 "interval" effect $F_{2,50}$=50.193, ***p*<0.001** "group × interval" effect $F_{4,50}$=0.461, p>0.05
Mixed two-way ANOVA (duration of traveling)	"group" effect $F_{2,25}$=0.252, p>0.05 "interval" effect $F_{2,50}$=31.331, ***p*<0.001** "group × interval" effect $F_{4,50}$=1.358, p>0.05
Mixed two-way ANOVA (duration of rearing)	"group" effect $F_{2,25}$=0.159, p>0.05 "interval" effect $F_{2,50}$=7.429, ***p*=0.001** "group × interval" effect $F_{4,50}$=0.84, p>0.05
Mixed two-way ANOVA (count of rearing)	"group" effect $F_{2,25}$=0.367, p>0.05 "interval" effect $F_{2,50}$=11.551, ***p*<0.001** "group × interval" effect $F_{4,50}$=0.797, p>0.05
Mixed two-way ANOVA (duration of grooming)	"group" effect $F_{2,25}$=1.218, p>0.05 "interval" effect $F_{2,50}$=2.494, p>0.05 "group × interval" effect $F_{4,50}$=0.736, p>0.05
Mixed two-way ANOVA (thigmotaxis)	"group" effect $F_{2,25}$=0.352, p>0.05 "interval" effect $F_{2,50}$=70.223, ***p*<0.001** "group × interval" effect $F_{4,50}$=0.11, p>0.05
Mixed two-way ANOVA (time spent in the center)	"group" effect $F_{2,25}$=1.416, p>0.05 "interval" effect $F_{2,50}$=7.138, ***p*=0.002** "group × interval" effect $F_{4,50}$=0.757, p>0.05
Mixed two-way ANOVA (entry to the center)	"group" effect $F_{2,25}$=1.453, p>0.05 "interval" effect $F_{2,50}$=2.111, p>0.05 "group × interval" effect $F_{4,50}$=2.925, ***p*=0.03**
One-way ANOVA (distance traveled)	0-5 min: "group" effect $F_{2,25}$=0.226, p>0.05 5-10 min: "group" effect $F_{2,25}$=0.353, p>0.05 10-15 min: "group" effect $F_{2,25}$=0.091, p>0.05

One-way ANOVA (duration of traveling)	0-5 min: "group" effect $F_{2,25}$=0.903, p>0.05 5-10 min: "group" effect $F_{2,25}$=0.251, p>0.05 10-15 min: "group" effect $F_{2,25}$=0.032, p>0.05
One-way ANOVA (duration of rearing)	0-5 min: "group" effect $F_{2,25}$=0.345, p>0.05 5-10 min: "group" effect $F_{2,25}$=0.398, p>0.05 10-15 min: "group" effect $F_{2,25}$=0.522, p>0.05
One-way ANOVA (count of rearing)	0-5 min: "group" effect $F_{2,25}$=0.566, p>0.05 5-10 min: "group" effect $F_{2,25}$=0.478, p>0.05 10-15 min: "group" effect $F_{2,25}$=0.374, p>0.05
One-way ANOVA (duration of grooming)	0-5 min: "group" effect $F_{2,25}$=, p>0.05 5-10 min: "group" effect $F_{2,25}$=, p>0.05 10-15 min: "group" effect $F_{2,25}$=, p>0.05
One-way ANOVA (thigmotaxis)	0-5 min: "group" effect $F_{2,25}$=0.113, p>0.05 5-10 min: "group" effect $F_{2,25}$=0.557, p>0.05 10-15 min: "group" effect $F_{2,25}$=0.581, p>0.05
One-way ANOVA (time spent in the center)	0-5 min: "group" effect $F_{2,25}$=1.205, p>0.05 5-10 min: "group" effect $F_{2,25}$=1.493, p>0.05 10-15 min: "group" effect $F_{2,25}$=1.097, p>0.05
One-way ANOVA (entry to the center)	0-5 min: "group" effect $F_{2,25}$=0.762, p>0.05 5-10 min: "group" effect $F_{2,25}$=3.012, p>0.05 10-15 min: "group" effect $F_{2,25}$=0.936, p>0.05
Rotarod	
Mixed two-way ANOVA (staying time)	"group" effect $F_{2,25}$=0.329, p>0.05 "trial" effect $F_{2,50}$=16.468, ***p*<0.001** "group × trial" effect $F_{4,50}$=0.096, p>0.05
Mixed two-way ANOVA (reaching speed)	"group" effect $F_{2,25}$=0.389, p>0.05 "trial" effect $F_{2,50}$=16.731, ***p*<0.001** "group × trial" effect $F_{4,50}$=0.099, p>0.05
One-way ANOVA (staying time)	trial 1: "group" effect $F_{2,25}$=0.54, p>0.05 trial 2: "group" effect $F_{2,25}$=0.274, p>0.05 trial 3: "group" effect $F_{2,25}$=0.084, p>0.05
One-way ANOVA (reaching speed)	trial 1: "group" effect $F_{2,25}$=0.551, p>0.05 trial 2: "group" effect $F_{2,25}$=0.296, p>0.05 trial 3: "group" effect $F_{2,25}$=0.162, p>0.05
Reciprocal social interaction	
One-way ANOVA (interaction time)	"group" effect $F_{2,16}$=0.161, p>0.05
Three-chamber social test – sociability trial	
Mixed two-way ANOVA (exploration time)	"group" effect $F_{2,20}$=0.157, p>0.05 "object" effect $F_{1,20}$=36.063, ***p*<0.001** "group × object" effect $F_{2,20}$=0.149, p>0.05
Paired *t*-test within each group stranger vs. empty cup	control: t_7=4.053, ***p*=0.005** vermis IV/V: t_6=3.947, ***p*=0.008** vermis VI/VII: t_7=2.986, ***p*=0.02**
One sample *t*-test within each group index vs. 0	control: t_7=4.43, ***p*=0.003** vermis IV/V: t_6=6.478, ***p*=0.001** vermis VI/VII: t_7=4.251, ***p*=0.004**
One-way ANOVA	"group" effect $F_{2,20}$=0.157, p>0.05

(total exploration time)	
Three-chamber social test – social novelty trial	
Mixed two-way ANOVA (exploration time)	"group" effect $F_{2,20}$=0.142, *p*>0.05 "object" effect $F_{1,20}$=15.205, ***p*=0.001** "group × object" effect $F_{2,20}$=1.185, *p*>0.05
Paired *t*-test within each group old stranger vs. novel stranger	control: t_7=-2.688, ***p*=0.031** vermis IV/V: t_6=-3.08, ***p*=0.022** vermis VI/VII: t_7=-1.041, *p*>0.05
One sample *t*-test within each group index vs. 0	control: t_7=3.684, ***p*=0.008** vermis IV/V: t_6=3.065, ***p*=0.022** vermis VI/VII: t_7=1.593, *p*>0.05
One-way ANOVA (total exploration time)	"group" effect $F_{2,20}$=0.142, *p*>0.05
Social recognition test – learning trial	
Mixed two-way ANOVA (exploration time)	"group" effect $F_{2,21}$=0.449, *p*>0.05 "object" effect $F_{1,21}$=39.115, ***p*<0.001** "group × object" effect $F_{2,21}$=0.307, *p*>0.05
Paired *t*-test within each group stranger vs. empty cup	control: t_7=3.522, ***p*=0.01** vermis IV/V: t_7=3.989, ***p*=0.005** vermis VI/VII: t_7=3.386, ***p*=0.012**
One sample *t*-test within each group index vs. 0	control: t_7=6.62, ***p*<0.001** vermis IV/V: t_7=8.388, ***p*<0.001** vermis VI/VII: t_7=5.105, ***p*=0.001**
One-way ANOVA (total exploration time)	"group" effect $F_{2,21}$=0.449, *p*>0.05
Social recognition test – testing trial	
Mixed two-way ANOVA (exploration time)	"group" effect $F_{2,21}$=0.224, *p*>0.05 "object" effect $F_{1,21}$=6.637, ***p*=0.018** "group × object" effect $F_{2,21}$=1.426, *p*>0.05
Paired *t*-test within each group old stranger vs. novel stranger	control: t_7=-4.668, ***p*=0.002** vermis IV/V: t_7=-0.899, *p*>0.05 vermis VI/VII: t_7=-0.588, *p*>0.05
One sample *t*-test within each group index vs. 0	control: t_7=5.483, ***p*=0.001** vermis IV/V: t_7=0.804, *p*>0.05 vermis VI/VII: t_7=0.114, *p*>0.05
One-way ANOVA (total exploration time)	"group" effect $F_{2,21}$=0.224, *p*>0.05
Object recognition test – learning trial	
One-way ANOVA (total exploration time)	"group" effect $F_{2,21}$=0.588, *p*>0.05
Object recognition test – testing trial	
Mixed two-way ANOVA (exploration time)	"group" effect $F_{2,21}$=2.194, *p*>0.05 "object" effect $F_{1,21}$=31.786, ***p*<0.001** "group × object" effect $F_{2,21}$=0.085, *p*>0.05
Paired *t*-test within each group old object vs. novel object	control: t_7=-3.022, ***p*=0.019** vermis IV/V: t_7=-3.544, ***p*=0.009** vermis VI/VII: t_7=-3.393, ***p*=0.012**

One sample *t*-test within each group index vs. 0	control: t_7=2.455, ***p*=0.044** vermis IV/V: t_7=3.934, ***p*=0.006** vermis VI/VII: t_7=3.952, ***p*=0.006**
One-way ANOVA (total exploration time)	"group" effect $F_{2,21}$=2.194, p>0.05
Chemogenetic manipulation – c-Fos imaging	
One-way ANOVA (c-Fos signal)	Acg: "group" effect $F_{2,15}$=5.027, ***p*=0.021** PL: "group" effect $F_{2,15}$=4.389, ***p*=0.032** IL: "group" effect $F_{2,15}$=6.454, ***p*=0.009** OFC: "group" effect $F_{2,15}$=1.122, p>0.05 ACC: "group" effect $F_{2,15}$=0.55, p>0.05 M1: "group" effect $F_{2,15}$=3.066, p>0.05 dSTR: "group" effect $F_{2,15}$=0.794, p>0.05 NAc: "group" effect $F_{2,15}$=0.041, p>0.05 RSD: "group" effect $F_{2,15}$=6.088, ***p*=0.012** RSG: "group" effect $F_{2,15}$=0.836, p>0.05 PtA: "group" effect $F_{2,15}$=2.433, p>0.05 TeA: "group" effect $F_{2,15}$=6.1, ***p*=0.012** Ect: "group" effect $F_{2,15}$=6.843, ***p*=0.008** PRh: "group" effect $F_{2,15}$=4.429, ***p*=0.031** lEnt: "group" effect $F_{2,15}$=1.228, p>0.05 CA1: "group" effect $F_{2,15}$=0.025, p>0.05 CA2/3: "group" effect $F_{2,15}$=0.295, p>0.05 DG: "group" effect $F_{2,15}$=0.223, p>0.05 CeA: "group" effect $F_{2,15}$=7.726, ***p*=0.005** BLA: "group" effect $F_{2,15}$=5.903, ***p*=0.013** BMP: "group" effect $F_{2,15}$=3.54, p=0.055 vTH: "group" effect $F_{2,15}$=1.522, p>0.05 mHA: "group" effect $F_{2,15}$=8.862, ***p*=0.003** VTA: "group" effect $F_{2,15}$=11.899, ***p*=0.001**
Post hoc Fisher's LSD test (c-Fos signal)	Acg: control vs. vermis IV/V: ***p*=0.024** vermis IV/V vs. vermis VI/VII: ***p*=0.01** PL: control vs. vermis IV/V: ***p*=0.044** vermis IV/V vs. vermis VI/VII: ***p*=0.013** IL: control vs. vermis VI/VII: ***p*=0.014** vermis IV/V vs. vermis VI/VII: ***p*=0.004** RSD: control vs. vermis IV/V: ***p*=0.004** vermis IV/V vs. vermis VI/VII: ***p*=0.023** TeA: control vs. vermis IV/V: ***p*=0.006** control vs. vermis VI/VII: ***p*=0.014** Ect: control vs. vermis IV/V: ***p*=0.008** control vs. vermis VI/VII: ***p*=0.004**

	PRh: control vs. vermis IV/V: ***p*=0.049** control vs. vermis VI/VII: ***p*=0.012** CeA: control vs. vermis VI/VII: ***p*=0.003** vermis IV/V vs. vermis VI/VII: ***p*=0.006** BLA: control vs. vermis VI/VII: ***p*=0.007** vermis IV/V vs. vermis VI/VII: ***p*=0.013** mHA: control vs. vermis VI/VII: ***p*=0.009** vermis IV/V vs. vermis VI/VII: ***p*=0.001** VTA: control vs. vermis IVI/V: ***p*=0.01** vermis IV/V vs. vermis VI/VII: ***p*<0.001**
One-way ANOVA (Pearson correlation coefficient *r*)	All regions: "group" effect $F_{2,825}$=11.588, ***p*<0.001** mPFC: "group" effect $F_{2,204}$=4.759, ***p*=0.01** ACC: "group" effect $F_{2,67}$=10.219, ***p*<0.001** Hippocampus: "group" effect $F_{2,204}$=28.224, ***p*<0.001** Amygdala: "group" effect $F_{2,204}$=4.371, ***p*=0.014**
Post hoc Fisher's LSD test (Pearson correlation coefficient *r*)	All regions: control vs. vermis IV/V: ***p*<0.001** control vs. vermis VI/VII: ***p*=0.001** mPFC: control vs. vermis IV/V: ***p*=0.004** control vs. vermis VI/VII: ***p*=0.017** ACC: control vs. vermis IV/V: ***p*<0.001** vermis IV/V vs. vermis VI/VII: ***p*=0.007** Hippocampus: control vs. vermis IV/V: ***p*<0.001** control vs. vermis VI/VII: ***p*<0.001** Amygdala: control vs. vermis VI/VII: ***p*=0.004**
Optogenetic manipulation – electrophysiology	
Paired *t*-test within each group light off vs. light on	BCs: AP frequency: t_6=-3.232, ***p*=0.018** PCs: AP frequency: t_8=3.794, ***p*=0.005** CV of inter-AP-interval: t_8=-8.419, ***p*<0.001**
Optogenetic manipulation – behavioral testing	
Social recognition test: Light ON during learning trial	
Learning trial	
Mixed two-way ANOVA (exploration time)	"group" effect $F_{2,19}$=4.692, ***p*=0.022** "object" effect $F_{1,19}$=55.301, ***p*<0.001** "group × object" effect $F_{2,19}$=1.446, *p*>0.05

Paired *t*-test within each group stranger vs. empty cup	control: t_7=3.913, ***p*=0.006** vermis IV/V: t_6=3.946, ***p*=0.008** vermis VI/VII: t_6=5.904, ***p*=0.001**
One sample *t*-test within each group index vs. 0	control: t_7=5.619, ***p*=0.001** vermis IV/V: t_6=4.808, ***p*=0.003** vermis VI/VII: t_6=7.244, ***p*<0.001**
One-way ANOVA (total exploration time)	"group" effect $F_{2,19}$=4.692, ***p*=0.022**
Post hoc Fisher's LSD test (total exploration time)	control vs. vermis IV/V: ***p*=0.042** vermis IV/V vs. vermis VI/VII: ***p*=0.008**
Testing trial	
Mixed two-way ANOVA (exploration time)	"group" effect $F_{2,19}$=10.918, ***p*=0.001** "object" effect $F_{1,19}$=22.39, ***p*<0.001** "group × object" effect $F_{2,19}$=1.341, *p*>0.05
Paired *t*-test within each group old stranger vs. novel stranger	control: t_7=3.387, ***p*=0.012** vermis IV/V: t_6=4.421, ***p*=0.004** vermis VI/VII: t_6=2.571, ***p*=0.042**
One sample *t*-test within each group index vs. 0	control: t_7=4.364, ***p*=0.003** vermis IV/V: t_6=5.665, ***p*=0.001** vermis VI/VII: t_6=2.6, ***p*=0.041**
One-way ANOVA (total exploration time)	"group" effect $F_{2,19}$=10.918, ***p*=0.001**
Post hoc Fisher's LSD test (total exploration time)	control vs. vermis IV/V: ***p*=0.005** vermis IV/V vs. vermis VI/VII: ***p*<0.001**
Social recognition test: Light ON during testing trial	
Learning trial	
Mixed two-way ANOVA (exploration time)	"group" effect $F_{2,22}$=1.593, *p*>0.05 "object" effect $F_{1,22}$=42.403, ***p*<0.001** "group × object" effect $F_{2,22}$=0.134, *p*>0.05
Paired *t*-test within each group stranger vs. empty cup	control: t_8=5.903, ***p*<0.001** vermis IV/V: t_7=4.404, ***p*=0.003** vermis VI/VII: t_7=2.443, ***p*=0.045**
One sample *t*-test within each group: index vs. 0	control: t_8=6.435, ***p*<0.001** vermis IV/V: t_7=5.714, ***p*=0.001** vermis VI/VII: t_7=2.032, *p*=0.052
One-way ANOVA (total exploration time)	"group" effect $F_{2,22}$=1.596, *p*>0.05
Testing trial	
Mixed two-way ANOVA (exploration time)	"group" effect $F_{2,22}$=3.352, *p*>0.05 "object" effect $F_{1,22}$=1.993, *p*>0.05 "group × object" effect $F_{2,22}$=7.828, ***p*=0.003**
Paired *t*-test within each group old stranger vs novel stranger	control: t_8=3.539, ***p*=0.008** vermis IV/V: t_7=0.277, *p*>0.05 vermis VI/VII: t_7=1.233, *p*>0.05
One sample *t*-test within each group index vs. 0	control: t_8=4.222, ***p*=0.003** vermis IV/V: t_7=0.361, *p*>0.05 vermis VI/VII: t_7=0.426, *p*>0.05
One-way ANOVA	"group" effect $F_{2,22}$=3.352, *p*>0.05

(total exploration time)	
Object recognition test: Light ON during testing trial	
Mixed two-way ANOVA (exploration time)	"group" effect $F_{2,23}$=0.086, p>0.05 "object" effect $F_{1,23}$=18.525, **p<0.001** "group × object" effect $F_{2,23}$=0.005, p>0.05
Paired *t*-test within each group old object vs. novel object	control: t_8=2.582, **p=0.033** vermis IV/V: t_7=2.343, p=0.052 vermis VI/VII: t_8=2.538, **p=0.035**
One sample *t*-test within each group index vs. 0	control: t_8=3.805, **p=0.005** vermis IV/V: t_7=3.707, **p=0.008** vermis VI/VII: t_8=4.089, **p=0.003**
One-way ANOVA (total exploration time)	Learning trial: "group" effect $F_{2,23}$=2.786, p>0.05 Testing trial: "group" effect $F_{2,23}$=0.086, p>0.05
Optogenetic manipulation – BDNF pathway imaging	
Social recognition test: Light ON during testing trial	
Learning trial	
Mixed two-way ANOVA (exploration time)	"group" effect $F_{1,10}$=1.09, p>0.05 "object" effect $F_{1,10}$=39.395, **p<0.001** "group × object" effect $F_{1,10}$=0.393, p>0.05
Paired *t*-test within each group stranger vs. empty cup	control: t_5=4.614, **p=0.006** nNOS-ChR2: t_5=4.365, **p=0.007**
One sample *t*-test within each group index vs. 0	control: t_5=6.293, **p=0.001** nNOS-ChR2: t_5=7.57, **p=0.001**
One-way ANOVA (total exploration time)	"group" effect $F_{1,10}$=1.09, p>0.05
Testing trial	
Mixed two-way ANOVA (exploration time)	"group" effect $F_{1,10}$=0.498, p>0.05 "object" effect $F_{1,10}$=7.364, **p=0.022** "group × object" effect $F_{1,10}$=6.451, **p=0.029**
Paired *t*-test within each group old stranger vs. novel stranger	control: t_5=2.712, **p=0.042** nNOS-ChR2: t_5=0.348, p>0.05
One sample *t*-test within each group index vs. 0	control: t_5=2.692, **p=0.043** nNOS-ChR2: t_5=0.18, p>0.05
One-way ANOVA (total exploration time)	"group" effect $F_{1,10}$=0.498, p>0.05
Open field: Light ON	
One-way ANOVA (distance traveled)	"group" effect $F_{1,14}$=1.071, p>0.05
Immunostaining of BDNF, TrkB, and pTrkB	
One-way ANOVA (BDNF expression)	PL: "group" effect $F_{2,15}$=2.375, p>0.05 CA1: "group" effect $F_{2,15}$=11.193, **p=0.001** CA2/3: "group" effect $F_{2,15}$=28.791, **p<0.001** DG: "group" effect $F_{2,15}$=1.442, p>0.05 BLA: "group" effect $F_{2,15}$=8.75, **p=0.003**
One-way ANOVA (TrkB expression)	PL: "group" effect $F_{2,15}$=3.157, p>0.05 CA1: "group" effect $F_{2,15}$=7.271, **p=0.006** CA2/3: "group" effect $F_{2,15}$=0.182, p>0.05

	DG: "group" effect $F_{2,15}$=4.845, ***p*=0.024** BLA: "group" effect $F_{2,15}$=9.334, ***p*=0.002**
One-way ANOVA (pTrkB expression)	PL: "group" effect $F_{2,15}$=11.566, ***p*=0.001** CA1: "group" effect $F_{2,15}$=4.136, ***p*=0.037** CA2/3: "group" effect $F_{2,15}$=1.933, $p>0.05$ DG: "group" effect $F_{2,15}$=29.953, ***p*<0.001** BLA: "group" effect $F_{2,15}$=4.594, ***p*=0.028**
Post hoc Fisher's LSD test (BDNF expression)	CA1: homecage vs. control: ***p*<0.001** homecage vs. nNOS-ChR2: ***p*=0.025** CA2/3: homecage vs. control: ***p*<0.001** homecage vs. nNOS-ChR2: ***p*<0.001** BLA: homecage vs. control: ***p*=0.002** homecage vs. nNOS-ChR2: ***p*=0.003**
Post hoc Fisher's LSD test (TrkB expression)	CA1: homecage vs. control: ***p*=0.046** homecage vs. nNOS-ChR2: ***p*=0.002** DG: homecage vs. control: ***p*=0.013** control vs. nNOS-ChR2: ***p*=0.022** BLA: homecage vs. control: ***p*=0.026** homecage vs. nNOS-ChR2: ***p*=0.001**
Post hoc Fisher's LSD test (pTrkB expression)	PL: homecage vs. control: ***p*<0.001** control vs. nNOS-ChR2: ***p*=0.005** CA1: homecage vs. control: ***p*=0.019** control vs. nNOS-ChR2: ***p*=0.002** DG: homecage vs. control: ***p*<0.001** homecage vs. nNOS-ChR2, ***p*=0.013** control vs. nNOS-ChR2: ***p*<0.001** BLA: homecage vs. nNOS-ChR2: ***p*=0.01**